LAWRENCE
LIVERMORE
NATIONAL
LABORATORY

UCRL-JRNL-206091

A Test of a Strong Ground Motion Prediction Methodology for the 7 September 1999, Mw=6.0 Athens Earthquake

L. Hutchings, E. Ioannidou, N. Voulgaris, I. Kalogeras, J. Savy, W. Foxall, G. Stavrakakis

August 17, 2004

Geophysical Journal International

A Test of a Strong Ground Motion Prediction Methodology for the 7 September 1999, M_w=6.0 Athens Earthquake

Lawrence Hutchings[**], Eleni Ioannidou[*+], Nicholas Voulgaris[+*], Ioannis Kalogeras[++], Jean Savy[**], William Foxall[**], and George Stavrakakis[++]

[+*]Department of Geophysics-Geothermics, University of Athens, Athens, Greece 15783; [*+] on leave of absence from the Ministry of Education, 2nd Gymnasium of Chalkida, Chalkida, Greece 11810

[**]Lawrence Livermore National Laboratory, Hazards Mitigation Center, Livermore, California 94551

[++]Institute of Geodynamics, National Observatory of Athens, Athens, Greece

July 4, 2004

Abstract

We test a methodology to predict the range of ground-motion hazard for a fixed magnitude earthquake along a specific fault or within a specific source volume, and we demonstrate how to incorporate this into probabilistic seismic hazard analyses (PSHA). We modeled ground motion with empirical Green's functions. We tested our methodology with the 7 September 1999, Mw=6.0 Athens earthquake, we: 1) developed constraints on rupture parameters based on prior knowledge of earthquake rupture processes and sources in the region; 2) generated impulsive point shear source empirical Green's functions by deconvolving out the source contribution of M<4.0 aftershocks; 3) used aftershocks that occurred throughout the area and not necessarily along the fault to be modeled; 4) ran a sufficient number of scenario earthquakes to span the full variability of ground motion possible; 5) found that our distribution of synthesized ground motions span what actually occurred and their distribution is realistically narrow; 6) determined that one of our source models generates records that match observed time histories well; 7) found that certain combinations of rupture parameters produced "extreme" ground motions at some stations; 8) identified that the "best fitting" rupture models occurred in the vicinity of 38.05^o N 23.60^o W with center of rupture near 12 km, and near unilateral rupture towards the areas of high damage, and this is consistent with independent investigations; and 9) synthesized strong motion records in high damage areas for which records from the earthquake were not recorded. We then developed a demonstration PSHA for a source region near Athens utilizing synthesized ground motion rather that traditional attenuation. We synthesized 500 earthquakes distributed throughout the source zone likely to have Mw=6.0 earthquakes near Athens. We assumed an average return period of 1000 years for this magnitude earthquake in the particular source zone, thereby having simulated a catalog of ground motion for a period of 500,000 years. The distribution of traditional ground motion parameters of peak acceleration or spectral ordinates then becomes the synthesized record from which we develop hazard curves in the form of the annual probability of exceedance. This approach replaces the aleatory uncertainty that current PSHA studies estimate by regression of empirical parameters from the worldwide database with epistemic uncertainty on what specific sources actually do at specific sites. This is a fundamental change for PSHA and eliminates the need to extrapolate current empirical data that was gathered over about 50 years to represent values for 10^{-3} annual probability of exceedance or less. This difference becomes especially significant for very sensitive structures that require estimates for 10^{-5} or less exceedance.

Introduction

The 7 September 1999, Mw=6.0 Athens earthquake occurred about 20 km from the center of Athens and at the western bounds of the greater metropolitan area. It was the first moderate-to-strong earthquake ever to have been reported at distances less than 30 km from the center of the metropolitan area (Makropoulos et al, 1989; Papazachos and Papazachou, 1997). About 100 buildings collapsed, which caused 143 casualties (Papadoppulos et al., 1999). Most damage was in areas surrounding the metropolitan center of Athens. The absence of strong historic seismic events had lead to the widely accepted conclusion of low seismicity for the greater area of Athens. Several strong motion recordings were obtained in central Athens, but no strong motion records were obtained from the high damage area to the northwest of Athens (Papadoppulos et al., 1999). A critical question is: what ground motion may have occurred in high damage areas of the 1999 earthquake? Also, what capabilities exist to predict the ground motion from future earthquakes, possibly closer to the center of Athens?

In this paper we test a physically-based methodology to predict the range of ground-motion that may occur from a particular magnitude earthquake along a specific fault or within a specific source volume, and demonstrate a means to incorporate this into traditional probabilistic seismic hazard analyses (PSHA). By "physically-based" we refer to a ground motion synthesis and prediction methodology that is based on physical understanding of the earthquake process. We choose two source volumes: the smaller being where the 1999 earthquake is considered to have occurred and the larger is where earthquakes of M_w=6.0 are considered capable of occurring near Athens. Figure 1 shows the two study areas, epicenter of the main event and locations of stations and events used to obtain empirical Green's functions in this study. We confine our study to M_w=6.0 events and utilize recorded strong ground motion from the 1999 event to evaluate our success. The test is at six sites. First, we test whether the actual ground motion recordings fall within the range predicted. The precise fault for the 1999 earthquake is not known, so we confine the calculations to a small source volume where the earthquake likely occurred, and run 63 scenario earthquakes. We compare actual values to predicted ranges of peak acceleration, absolute acceleration response spectra, Fourier amplitude spectra, and duration obtained by in the likely source volume. We used the method of Anderson (2003) that compares seismograms on

ten criteria over 5 frequency bands to test whether one of our models provides ground motions that match observed time histories. In this paper we are only considering linear response ground motion. The records we use in the study occurred on competent enough geology, or had low enough values to be considered a linear response. We found that the "best fitting" rupture models are consistent with rupture characteristics identified by independent investigations. This is important because it demonstrates that our ground motion synthesis approach gives the right answer when actual physical parameters of rupture are known. Then, predictions can be made from physical rupture parameters that can be estimated in advance of an earthquake, and bounded by knowledge of the earthquake process. Finally, we synthesize ground motion is areas that had damage from the 1999 earthquake, but which did not have strong motion recordings.

We also developed a demonstration PSHA for a source region near Athens utilizing synthesized ground motion rather than traditional attenuation relations (peak acceleration or response spectral ordinates). We synthesized 500 earthquakes distributed throughout a source volume likely to have Mw=6.0 earthquakes near Athens. We assumed an average return period of 1000 years for this magnitude earthquake in the particular source zone, thereby having simulated a catalog of ground motion for a period of 500,000 years. The distribution of traditional ground motion parameters of peak acceleration or spectral ordinates then become a simulation of the actual record of ground motion for this time period from which we develop hazard curves in the form of the annual probability of exceedance.

Current PSHA methods were developed in large part to meet licensing needs for nuclear power plants. In this application annual probabilities of exceedance of ground motion measures of interest (e.g. peak and spectral accelerations or spectral velocities) are in the range of 10^{-3} to 10^{-4}. Since the recurrence intervals of the dominant contributing earthquakes are generally in the range of a few hundred to a few thousand years, the ground motion estimates are generally sampled from the central region of the probability distributions on the ground motion attenuation relationships, or at most from the beginnings of the tails of the distributions. However, licensing practices for sensitive structures that require estimation of ground motions with annual probabilities of exceedance on the order of 10^{-5} to 10^{-7} inevitably lead to sampling the virtually unconstrained tails of the ground motion probability distributions. This results in estimates of ground motion that can be extremely high and that are believed to be physically unrealizable. However, there is at present no generally accepted method either to better characterize the tails

of the distributions or to truncate them at some upper bound ground motion value. We show that a physically-based approach to PSHA naturally defines the shape of the tails of the distribution and bounds the ground motion.

Our basic approach to compute ground motions is to simulated finite rupture models with the Green's function summation solution of the representation relation (Aki and Richards, 1980). In this approach, Green's functions for each portion of the fault are calculated and convolved with source functions at each point along the rupture surface. Generally, at long periods (1 second and above) the Green's function solution can be obtained by purely numerical techniques such as finite difference or finite elements, since at these periods only coarse spatial resolution is needed in source and geological models. At short periods, where the geology cannot be modeled numerically, empirical Green's functions, constrained random vibration Green's functions, or empirically constrained numerical Green's functions can be used to capture the full short-wavelength complexity in source and path. In this study we synthesize ground motion from 1.0 to 20.0 Hz and use empirical Green's functions. We obtain the empirical Green's functions from recordings of aftershocks and background seismicity with magnitudes M<4.0, and they are not necessarily on the faults to be modeled. We do not synthesize low frequencies that would utilize synthetic Green's functions. All the necessary elements to conduct PSHA studies with synthesized ground motion are in place and only need to be implemented in a systematic way to capture the epistemic and aleatory uncertainty.

Physically-based Probabilistic Hazard Approach

Historically, strong ground motion prediction has generally taken one of two paths: probabilistic or deterministic. Here we have combined the two methods into a new approach for probabilistic seismic hazard studies. Following Cornell (1968) and (Stepp et al., 2001), probabilistic seismic hazard analyses require: 1) an interpretation of seismic sources that constitute a hazard to a particular site from which the distances of earthquakes from the site can be determined; 2) an interpretation of earthquake recurrence for each source; 3) an evaluation of ground motion attenuation for the region. The ground motion attenuation relationships are simple functions of earthquake magnitude and source-site distance (and in some cases a few additional source parameters) and are empirically derived from the strong motion database recorded from past earthquakes worldwide. And, (4), given the input evaluations, the PSHA method integrates

over all values of the variables and produces and estimate of the mean yearly frequency of exceedance of ground motion amplitude at the site, i.e. a hazard curve.

Both earthquake source models and ground motion attenuation relationships are subject to significant uncertainties, which are expressed as probability distributions (giving an estimate of the median and standard deviation) on earthquake occurrence rates and on the ground motion relationships. The uncertainty in a ground motion relationship arises from the variability in source characteristics among events of the same size in the strong motion database and from the different earth structures through which the seismic waves from the events propagated. In PSHA studies this is considered aleatory uncertainty, the uncertainty due to inherent randomness of the process. Current PSHA studies are based upon the ergodic assumption that the randomness in space form several sources is the same as the randomness in time from the same source (Anderson and Brune, 1999). With the ergodic assumption, correlation between the ground motion and the specific source, path, and site is lost, thereby leading to potentially higher total uncertainty in hazard estimates than if each earthquake source release of energy were individually propagated to the site of interest. There is also an attempt to model epistemic uncertainty, the uncertainty in knowledge about the earthquake processes. This refers to factors such as strike, dip, slip vector, ect., that could further reduce aleatory uncertainty if they were known and included as regression parameters.

Alternatively, a deterministic approach identifies significant faults or source zones and establishes the Maximum Possible Earthquake (MPE), as for PSHA; Design Operating Earthquake (DOE), essentially the mean of PSHA; and the Operating Basis Earthquake (OBE), maximum during lifetime of facility. Deterministic hazard studies have had the problem of identifying the appropriate source for each earthquake and their likelihood of occurrence, and PSHA has had the problem of too short of history of recorded data and accurately accounting for epistemic uncertainty of the source and propagation of strong ground motion. In this paper we incorporate the combination of deterministic studies by calculating actual earthquake rupture and recorded ground motion relevant to a particular site, and incorporate this into PSHA studies by replacing the use of attenuation relations. The output from this PSHA approach is a library of source- and site-specific ground motion time series that would comprise a sample of all the earthquakes that could affect a site during its design life. These seismograms are then used to either develop hazard curves of traditional engineering parameters in the form of the annual

probability of exceedance, or used directly into building design to develop risk estimates. This approach replaces the aleatory uncertainty that current PSHA studies estimate by regression of empirical parameters from the worldwide database with epistemic uncertainty on what specific sources may actually do at specific sites. The uncertainty of the PSHA is bounded by defining bounds on the physical parameters that go into the computation of ground motion, rather than having an unbounded PSHA developed from unbound shapes to probability distributions.

Intensity and Damage to Engineering Structures

Figure 2 shows the isoseismal intensity from the 1999 Athens earthquake as it has been compiled after Protonotarios (1999) and Ioannidou et al (2001). Also, shown on Figure 2 are names and locations of stations used in this study, and they are listed in Table 1. Most of the damage occurred within about a 10 km diameter area, centered about 10 Km northeast of the epicenter. However, projection up-dip of the proposed fault plane (and hypocenter) would intersect near the high damage area. Severe damage decreased rapidly with the distance from the center of damage, and in most areas of Athens damage was non-structural and consisted mainly of cracks to in-fill brick walls. All classical monuments survived the earthquake without significant damage (EERI, 1999). Small rotations of some columns and the fall of small pieces of marble were reported for the Acropolis of Athens, but were considered of minor importance by the archaeologists. No damage was reported on highways, roads or railroad tracks, except for cracks and minor landslides on the road leading to the summit of Parnitha Mountain, near the epicenter. Underground pipelines were apparently undamaged. The recently constructed natural gas network did not suffer any damage at all, although it crosses the mezoseismal area at a shallow depth. No damage was reported to the new underground metropolitan railway. The Mornos duct-way, which supplies Athens, suffered no damage, although it runs almost parallel to the Aspropyrgos fault and through the mezoseismal area.

Predicting a Range of Ground-Motions with a Physically Based Model

We utilize a physically based kinematic source model to generate rupture scenarios that span the variability of potential ground motion in a predictive situation. The basic premises of the methodology are: 1) accurate synthesis of recorded ground motions for a particular fault rupture scenario, sufficient for engineering purposes, is possible, 2) a general description of the rupture is sufficient for synthesizing realistic ground motions; 3) the rupture characteristics of a fault can be constrained in advance of possible future rupture by interpreting physical properties such as

geologic structure, seismicity, and tectonics of the region, 4) the range of possible fault rupture scenarios is narrow enough to functionally constrain the range of strong ground motion predictions, and 5) a discrete set of rupture scenarios is sufficient, for engineering purposes, to span the infinite combinations possible from a given range of rupture parameters. An important corollary is that if a scenario earthquake matches observed seismograms, then the rupture parameters of that scenario are close to what actually happened.

Physically based here refers to models that are consistent with the elastodynamic equations of seismology and fracture energy, and they are consistent with physical understanding of how earthquakes rupture, laboratory experiments, numerical modeling, and field observations of earthquake processes. These models are often referred to as quasi-dynamic models (Boatwright, 1981). Our source model is one but a family of such models; others include Boatwright (1981), Hartzell (1982), Heaton (1982), Papageiorgiou and Aki (1983), Spudich and Frazier (1984), Cohee et al. (1991), and Mariagiovanna et al. (2003). In a true probabilistic seismic hazard study all physically based kinematic models would be employed to capture the full epistemic uncertainty of the problem. Here we employ the source model of Hutchings (1991 and 1994), and further refined in this paper. Physically based source models allow one to vary input parameters and generate combinations that have not yet occurred in nature. Bounds on input parameters are based upon physical understanding and naturally bound the synthesized ground motions.

Our basic premise is that fifty years of strong motion records is insufficient to capture the range of site and propagation path conditions, rupture processes, and geometric relationships between source and site that are possible from earthquakes. Ground motion syntheses approaches that are based upon regression of the empirical database have the same problem as empirical attenuation relations. Such models have little or no physical bases but have been tested and adjusted to fit of the observations available. These models can only model what happen in the past. This includes models that fit target spectra obtained from regression with the empirical database, and those that rely on scaling relations between large and small earthquakes. The ultimate solution for modeling earthquakes would be dynamic solutions that satisfy elstodynamic equations and fracture energy and have known elastic constants and constituent relations for the faulting process. However, these parameters are very uncertain in the fault zone, several poorly bounded assumptions need to be used, and resultant uncertainties in computations make there

usefulness limited to better understanding the earthquake process and providing bounds for kinematic rupture models.

The range of ground motion calculations is implement by the computer programs EMPSYN (Hutchings, 1988 and Hutchings et al., 2003) for ground motion simulation and HAZARD (Hutchings et al., 1996) for generating scenario earthquake models. EMPSYN numerically solves the representation relation (Aki and Richards, 1980). Rupture parameters include rupture geometry, hypocenter, rupture roughness, rupture velocity, healing velocity, slip distribution, asperity size and location, and slip vector. Scenario here refers to specific values of these parameters for a hypothesized earthquake, and the program HAZARD randomly generates these. Synthetic strong ground-motions are then generated for each rupture scenario. A sufficient number of scenarios are run to span the variability in strong ground motion due to the source uncertainties. In this paper we ran 63 scenarios for the source volume hypothesized to be where the 1999 earthquake occurred, and 500 scenarios in the larger source zone where magnitude Mw=6.0 earthquakes are likely to occur.

EMPSYN numerically computes the discretized representation relation, and it utilizes the form (Hutchings and Wu, 1990 and Hutchings, 1991):

$$u_n(X,t) = \sum_{i=1}^{N} \frac{\Delta_i A_i S(t-\tau_i)}{M_{0i}^e} \quad e_n(X,t-\tau_i) \tag{1}$$

This is an exact solution for the representation relation under certain conditions, and it is our intent to keep as close to the mathematically exact solution as possible, with approximations adding to the uncertainty of the solution. The fault rupture surface is divided in N small areas A_i such that $\sum A_i$ equals the total rupture area. $e_n(X,t-\tau_i)$ is the empirical Green's function for the i^{th} element obtained from recordings of small earthquakes. u_n has the same units as e_n. At this point the focal mechanism solution of the large and small event are assumed to be the same, and the small event is assumed to have a step dislocation source time function (discussed further below). e_n provides the elastodynamic Green's function ($G_{np,q}$) in the conventional representation relation (see Hutchings and Wu, 1990). $G_{np,q}$ is isolated from the empirical Green's function by deconvolving out the source function (discussed below) and normalizing by the scalar seismic

moment of the small event M_{0i}^{e}. The disconvolution with the source function of the small earthquake is included in the analytical solution for the slip function of the larger event. Therefore, $S(t)_i$ is the desired slip function analytically deconvolved with the step function, and t is time at the element and it is equal to 0.0 at the arrival time of the rupture front. Empirical Green's functions are interpolated to have a source at each element and are adjusted to have origin time when t is 0.0. $\overline{r_i}$ is the radial distance from the hypocenter to the elemental source, and V is the rupture velocity. The main advantage of the empirical Green's function approach is that if e_n is managed properly, then it provides the exact elastodynamic Green's function for the real earth.

We utilize the Kostrov slip function in EMPSYN. It was derived from the analytical solution for rupture of a circular crack in a homogeneous medium (Buridge and Willis, 1969):

$$K(X,t) = \frac{0.81}{}\left[\right]^{2} \quad (2)$$

Where X_i^2 is position vector from the hypocenter, t' is relative to origin time of the earthquake, V_r is rupture velocity, β is shear wave velocity, c is a constant equal to 0.81 for V_r equal to 0.9β, u is rigidity, and a is stress drop. This expression does not include healing or termination of the slip. We transform the Kostrov function is transformed to be relative to element time, t_i' is zero at the arrival time of the rupture front:

$$t = t - t \quad (3)$$

where t is the rupture time from the hypocenter. $/V_r$ in equation 2 has been replaced by t to allow for variable rupture velocity. Making this transformation to 2 and adding healing, the Kostrov slip function at an element become:

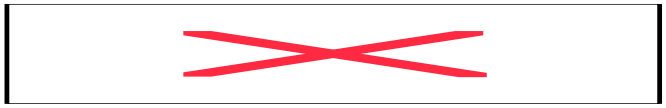

(4)

for time at the element from 0.0 to $_i$ and constant after that; where $_i$ is the rise time at the i^{th} element, and $\frac{1}{H(t)}\oplus$ is the deconvolution with the step function. The rise time in EMPSYN is determined by the shortest time for the rupture front to reach the fault edge and a healing phase to then reach the element. Now, t puts a rupture distance dependence on equation 4, and for long faults it causes $S(t')_i$ to increase with spatial separation from the hypocenter. To constrain this, t is limited to be equal to or less than the rupture time to the nearest edge, but not less than 1.0 sec. We equate this limiting value to a "memory" of fault rupture and a departure from a pure crack solution for an extended rupture.

EMPSYN utilizes a summation of step functions to model the Kostrov slip function in the time domain. The time delay for the step functions' summation is at the digital sampling rate of the empirical Greens functions to insure that high frequency artifacts are higher than the frequency range of interest. In the frequency domain EMPSYN employs a ramp function with all the parameters of the Kostrov slip function. Hutchings (1994) showed that the difference in computed seismograms using the ramp to model the shape of the Kostrov slip function was indistinguishable in the frequency range of interest.

Recordings of effectively impulsive point source events are used as Green's functions for each elemental area. All available recordings of small earthquakes are used as empirical Green's functions and interpolated to provide the Green's function for each element. This modeling approach only requires that the number of times small earthquakes are used in the synthesis be such that the sum of their moments adds up to the moment of the large earthquake. Therefore,

low frequency amplitudes match those of observed seismograms. The high frequency is matched simply by using appropriate rupture parameters (Hutchings, 1994).

Data and Site Conditions

Main shock records and recordings of aftershocks used to obtain empirical Green's functions are described in Ioannidou (2001). Fifteen strong-motion accelerograph stations recorded the main shock near and around Athens. The peak ground accelerations ranged from 0.05 to 0.5 g. Table 1 lists stations used in this study. NOAIG data were recorded by their permanent strong motion array and Attico Metro S. A. instruments. The procedure for processing strong motion records of NOAIG is based on the standard procedure of the CALTECH Institute (Trifunac and Lee, 1973), and is described, in detail, by Stavrakakis et al. (1993). We synthesized observed records at ATHA, DMKA, FIXA, THVC, SGMA, and SPLA for this study. Two additional sites could have been used, but were not: SGMB, which is located just 19 m below SGMA, and SPLB, which is at the same depth and geology as SPLA, but 150 m distant. SPLB is in the basement of a three-story steel structure. These are the only sites that had recordings of small earthquakes that could be used for empirical Green's functions. The records used in this study ranged from 0.05 to .2 g for all stations except SPLA, and are not considered to be in the non-linear response range. Figure 9 shows the recorded accelerograms. Station SPLA is on competent soil and may have had non-linear response, but the observation that its records are modeled as well as other stations suggests that it did not.

The UoADGG deployed two types of stations during the installation of a temporary network to record aftershocks. These sites were largely in the area of high damage, but none was at a location where the main event was recorded. Acceleration was recorded at sites PEFK and COUR, situated within the center of the network, using Kinemetrics ETNA instruments. The previously mentioned procedure for processing strong motion accelerometer records was applied on the data from these stations. At the NEOK, STEF, MAGO, FILI, PSAR and ZOFR sites RefTec recording instruments were installed. The first four of these were equipped with the LE-3D 1Hz Lennartz sensor while the last two stations were connected to GURALP CMG 40-T broadband seismometers. The records obtained were instrument response corrected according to the sensor specifications to obtained velocity time histories, and they were differentiated to provide accelerograms. The geology of all these sites is on competent geology and non-linear response is not expected for the level of ground motion considered.

Figure 3 shows the geology of the study area and Table 1 describes categories of recording site geologic conditions as discussed in Ioannidou et al (2001): (a) hard rock formations, dolomites or limestone of U. Triassic to L. Jurassic age and limestone of U. Cretaceous age; (b) rock - soft rock formations, slightly to medium weathered phases of the Athens Schist, metamorphosed schist and limestone, cohesive talus cones and medium to well cemented conglomerates or Neogene marls; (c) soil - stiff soil formations, moderately thick weathering products of the geological bedrock, alluvium deposits of medium to high density or recent man-made deposits. The geology of the sites is primarily shales, sandstones, crystalline limestones, and soil conditions from firm soil to alluvium. Most of the recording sites lay in the vicinity of major infrastructure, having been constructed in the past or being under construction at the time of the earthquake, i.e. the surface or underground stations of the Athens Subway (DFNA, FIXA, PNTA, SGMA, SGMB, SPLA, SPLB).

Table 2 lists source parameters of the main Athens earthquake reported by a number of Institutions. Estimated epicentral locations were fairly well constrained (excluding Harvard's), but depths ranged from approximately 8 to 17 km. Focal mechanism solutions are in an overall agreement corresponding to an extensional a WNW-ESE trending nodal plane dipping to SW. Papadopoulos et al (2000) interpreted the aftershock distribution as a zone striking WNW- ESE with a length of 25-30km, dipping 80^o SW. However, the variations of focal parameters, location differences and absence of surface trace, do not permit association with a particular fault. There was no apparent surface rupture. Secondary, gravitational fissures, small ground cracks, minor landslides and falling rocks have been mapped in the vicinity of the village of Fili (Figure 2), consistent with active features striking N 120^o - 130^o, dipping 70^o - 80^o SW with rake angle of 76^o to 88^o (Pavlidis, 2000). Teleseismic inversion of body waves (Papadimitriou et al, 2000; Louvari and Kyrazti, 1999) estimate the depth of the main event at 8 and 11 km, respectively, with a source duration of about 5 sec releasing most energy in the first few seconds. Additional detailed seismological information about the earthquake can be found in Stavrakakis (1999).

Source Parameters of Aftershocks

We estimated critical source parameters of aftershocks that provided empirical Green's functions. We conducted a simultaneous inversion of recordings of aftershocks to obtain source moment (M_0) and corner frequency (f_c), and site-specific kappa (K) using the computer program NetMoment (Hutchings, 2002). This study is similar to that presented in Ioannidou et al

(2001) except that we incorporate whole path K together with site specific K in the calculations, and we only used stations without a significant site response in the inversion. Stations identified from the Ioannidou et al study that did not have a significant site response are underlined in column one of Table 1. The joint inversion is based upon the assumption that for a particular earthquake, moment and the source corner frequency will have the same value when calculated from spectra at each site; so that differences in spectra are due to site response, propagation path K and individual site K.

Prior to the joint inversion spectra are scaled for moment (Aki and Richards 1980, pg. 116) by:

$$\Omega'(f) = \frac{4\pi R \rho_x^{1/2} \rho_\xi^{1/2} \beta_x^{1/2} \beta_\xi^{5/2}}{S^S F^S} U(f) \exp(\pi f t_r^*) \qquad (5)$$

where $U(f)$ is the recorded displacement spectra at station i, $R^{.9}$ is correction for geometrical spreading for distances less than 30 km for Italy (Malaganini et al., 2000), ρ_x is density at the station and ρ_ξ is density at the source, β_x is shear velocity at the station and β_ξ is shear velocity at the source. A one-dimensional velocity model is used. ***S*** and ***F*** are the free surface correction and focal mechanism correction, respectively. The free surface correction is determined from the velocity model using the reflection coefficients as outlined in Aki and Richards (1980, pg. 190). The focal mechanism solution is not available for most of the events, so an average focal mechanism correction factor for S-waves of 0.63 was used. Density is determined from the P-wave velocity by the linear relation: $\boldsymbol{\rho}$ = (a-0.35)/1.88 (Lama and Vutukuri, 1978). $\boldsymbol{\rho}$ = 2.37 gm/cm^3 is the surface density and is based upon near-surface P-wave velocity of 4.1 km/sec. It is assumed that the long period waves used to calculate moment primarily sample the average regional geology. $\boldsymbol{\rho}$ varies with the depth of the event, and $\boldsymbol{\rho}$ = 3.16 gm/cm3 at 15 km depth for this study..

The Fourier amplitude spectra were fit to the modified Brune source spectra for a particular event:

$$\Omega(f) = \frac{M_0 \exp(-\pi f t_g^*)}{\left(1 + \left(\frac{f}{f_c}\right)^2\right)} \tag{6}$$

where M_0 is the moment, f is the frequency, f_c is the source corner frequency, and K_i is site specific kappa value at station i.

Seismograms were rotated to radial and transverse components, and the vertical and radial were square-of-sum-squared added to get one Sv spectrum, then the Sv and Sh components were scaled with the terms in of equation 5 and averaged before the inversion. Corrected spectra were fit to equation 6 by fitting frequencies from 1.0 to 20.0 Hz for most stations; some stations had noise such that they were fit to a broader or narrower bandwidth. The best fitting combination of the free parameters (M_0, f_c, K_i) was found by iteration from a starting model using the Simplex algorithm (Cacceci and Cacheris, 1984; Nelder and Mead, 1965; Numerical Recipes, 1998, Chapter 10.4).

The fit to K and f_c are dependent upon the long period spectral level and in a simultaneous inversion this can result in a bias. For example, if a site has a factor of 2 greater long period spectral levels than the solution for the joint inversion, and is forced to fit the site-specific high frequency, then the K value will be higher and the f_c will be lower than if spectra were fit individually. Therefore, in an effort to get unbiased values of K and f_c we normalized spectra to have the same long period spectral level (average of all recordings for a particular event), then conducted the simultaneous inversion. This did not affect the moment calculation significantly because K generally has minimal effect at these periods and the spectral fit of the inversion is primarily the mean of long period values anyway. This inherently adds the assumption that at the longest periods, site response is not a factor. Table 3 lists the source parameters determined and number of aftershocks used in the inversion. Figure 4 shows fits to observed spectra for several events. The differences in shapes of individual spectra are due to site specific K. The solid line shows the modified Brune model over the frequency band utilized. The actual moment is the

projection of this fit to DC frequency. The error analysis of moment calculations is discussed below in "Error Analysis".

Empirical Green's Functions

We use the definition of empirical Green's functions (EGFs), as outlined by Hutchings and Wu (1990), to be recordings of effectively impulsive, point, shear sources. "Effectively impulsive, point, shear" sources here refers to the observation that factors such as rise time, rupture duration, or source dimension are small enough that their effect cannot be observed in the frequency band of interest. Also, stress drop changes are reflected only in the differences of seismic moment. As such, their source spectra are flat up to the highest frequency of interest, 20 Hz in this study, and scale only linearly for differences in seismic moment. Hutchings and Wu found that below a moment threshold of about 1.5×10^{21} dyne-cm (depending on the recording site) events satisfy the point, shear, source criteria, and all spectra and time series at a particular station had essentially the same shape and waveforms and scaled linearly in amplitude only for differences in moment.

In this study most events used have moments greater than the threshold identified by Hutchings and Wu. Here we utilize the output of the source parameter study to deconvolve out the Brune source from the recordings to create EGFs. We confine this approach to events with magnitude < 4.0 to minimize finite source effects and keep the basic assumption of the Brune source model. This extends the synthesis methodology of Hutchings and Wu (1990) to include events larger than those that satisfy the criteria of being effectively impulsive, point, and shear source earthquakes. The Brune source has zero phase shifts so that in the deconvolution only the amplitude spectra are affected. There is no apparent non-causal effect in time series due to the deconvolution. Figure 5 shows several recordings that have been corrected to provide effectively impulsive, point, shear source event recordings (EGFs). The time series are in acceleration, and their displacement spectra are shown. The observation that the spectra are not flat after the deconvolution is assumed to be due to effects of attenuation and site response (fmax effect).

It is not possible to record empirical Green's functions from all locations along a fault of interest and with the same focal mechanism solution, so that source locations of empirical Green's functions have also been interpolated to fill in the fault. In this study, source events for empirical Green's functions are distributed throughout the area and do not necessarily occur on the fault to be modeled. In this application the empirical Green's functions carry the average

propagation prosperities of the area and site-specific site response. Previous studies have shown that it is not necessary to have source events fall directly along the fault of interest. The spatial dependence of empirical Green's functions has been researched by Hutchings and Wu (1990) and they found that the variability in ground motion due to differences in source location and/or focal mechanism solutions are much less than that due to the site response, and Hutchings (1991), Hutchings (1994), and Jarpe and Kasameyer (1996) found that interpolation for different source locations along a fault works quite well. Wossner et. al (2002) found that the number of empirical Green's functions affects the amplitude of synthesized seismograms. They found that amplitudes in the synthesized records, for frequencies higher than the source corner frequency, generally tend to be higher for records that use a single EGF interpolated over the fault, and they achieved more stable, and reliable results, if at least five EGFs are used. In synthesis, we have the option of correcting for different focal mechanism solutions, but Hutchings and Wu (1990) and Jarpe and Kasameyer (1996) found that for high frequencies it does not improve the synthesis. Interpolation is performed by correcting for attenuation, geometrical spreading, and P- and S-wave arrival times due to differences in source distances as discussed in Hutchings and Wu (1990).

Previous Validations

The prediction methodology has previously been tested. First, the computer code EMPSYN has been validated by synthesizing an idealized earthquake with the same parameters as was used by similar syntheses approach conducted at UCSB (Peng-Cheng Liu, personal communication, 1999). Their results were essentially identical. Hutchings (1994) also synthesized an expanding circular crack solution and matched the analytical solution. Jarpe and Kasameyer (1996) performed a systematic validation of the modeling approach using Loma Prieta earthquake data. They fixed the moment, focal mechanism solution, slip distribution, and geometry from independent studies, and modeled the observed strong ground motion at 26 sites. They found that the standard error between observed and predicted response spectra is less than or equal to other methods for periods 0.05-2.0 s and is significantly less than regression methods based on pre-Loma Prieta empirical strong-motion data at periods between 0.5 and 5.0 sec.

Hutchings (1991) included the variability resulting from not knowing the source by modeling several rupture scenarios along a segment of the fault, and for a particular moment. Hutchings (1991) "predicted" strong motion parameters of peak acceleration and pseudo-velocity

response at five sites that recorded the Loma Prieta earthquake. Hutchings utilized 25 rupture scenarios along the fault where the Loma Prieta earthquake occurred to account for the source variability from not knowing the source prior to the occurrence of the earthquake. The engineering parameters were predicted within the 16 and 84% lognormal standard errors at four of the five sites. The fifth site had recorded motion just above the one standard error value for both peak acceleration and pseudo-velocity response. Other tests and validations include Hutchings (1994), Foxall et al., (1994), Hutchings et. al (1997), Hutchings et. al (1998), Scognamiligo (2004).

Fault Rupture Model Constraints

Here we use knowledge about how earthquakes rupture to estimate bounds of possible rupture parameters that may have been identified prior to the 1999 earthquake. Rupture parameters are then selected by a Monte Carlo pick using a triangular distribution between limits. The limits of input parameters will naturally bound the range of synthesized ground motions. Also, because input permeates are correlated through a physical model, unrealistic combinations that can't happen in nature are excluded. Here, general limits as obtained in the literature are utilized. Certainly a major area of research in the future is in identifying the physical limits to input parameters in order to get the physical range of ground motion possible (Bommer et al., 2004).

Moment: The moments listed in Table 3 show about a factor of two variation in estimates for the 1999 earthquake, from 7.8 to 17.0 $x10^{24}$ dyne-cm, and the resulting moment magnitudes range from 5.9 to 6.1, respectively. The average of moments from Table 3 is $1.19x10^{25}$ dyne-cm. We use $1.122x10^{25}$ dyn-cm for this paper, which is moment magnitude 6.0 using the Hanks and kanamori (1979) relation.

Hypocenter: Hypocenter limited to be greater than 0.2 km from fault edge to avoid stress discontinuities and strains that exceed 10^{-1}. Depth is limited to be within the lower half of rupture area, as large earthquakes are theoretically predicted to nucleate at depth (Sobson, 1982, and Tse and Rice, 1986). Scenario earthquake ruptures range from 0.0 to 25.0 km to keep them with the brittle crust. However, no surface rupture is allowed, as has not been observed in the geologic record for the region.

Strike: The Kifissos and Aegaleo fault zones to the eastern part of the selected area trend NE - SW, while Thriassion fault zone to the center and west of the epicentral area trends WNW-ESE.

To the west part of the later zone W-E faults are also apparent, coinciding with the direction of the extensional faults of the seismically active, major graben structure of the Corinthian gulf further west. The morphological expression of the Thriassion Pedion fault is identifiable in aerial photographs and satellite images. To the north of the Thriassion Pedion fault, smaller faults with similar strike direction span the block of Parnitha Mountain. From this, and consideration of uncertainties of strike at depth, we limit the strike of possible rupture to be between N100^o E and N125^{o}E.

Slip Vector: Today, the extension character in the area is prominent, leading us to limit the rupture to normal or oblique slip, although due to the kinematic complexity of the structures reverse or thrust faults were, almost certainly present in the past. (Mariolakos I et al, 2000). From this we limit the slip vector to be from -70^o to -110^o. However, the slip vector values are only used for EGF's that have a focal mechanism solution. If no focal mechanism solution is available an average value of 0.63 was used for the S-wave correction factor.

Dip: The dip was limited to range from 35.0^o to 55.0^o, following the same argument as to the slip vector.

Fault Rupture Geometry: Fault shapes are constrained to be elliptical. Examination of slip distributions of previous earthquakes shows that rectangular ruptures generally only occur on faults that rupture through the entire crust; thereby they have a general elliptical shape (Hartzel, many references; Wald, many references). The length of the major axis for this study is constrained to vary from 7 to 13 km, and the eccentricity varies from 0.0 to 0.90, which limits the minor axis to be between about 5 to 11 km. This resulted in the fault area ranging from about 40 to 110 km^2, with an average area of 93 km^2. The average area of rupture models is 90.6 km^2. This compares to 93 km^2 that Wells and Coppersmith (1994) and 79.9 km^2 that Somerville et al (1999) obtained for Mw=6.0 earthquakes by regression of all earthquakes in their data set.

Slip distribution: The slip distribution is varied in two ways. First, the Kostrov slip model with healing (Hutchings, 1994) has variable rise time and slip amplitude on the fault, but constant stress drop. This results in portions of the fault with high slip amplitude. Second, Smaller areas with high slip amplitudes and high stress drop are modeled. These are called asperities. Asperities are not allowed to overlap. Fault displacement for asperities grade from the value of background rupture at the edge to greatest at the center. We used the definition of an asperity as defined by Somerville et al (1999) to examine slip distribution. Somerville et al used inversion

results, primarily from Hartzell and/or Wald (many references), to characterize slip distribution as that which has an average slip greater that 1.5 times the overall average slip amplitude. Our slip models had an average of 20% with slip greater then 1.5 times average slip and this Somerville has 20.67% from regression with all their data.

Slip amplitude values, with or without asperities, are allowed to vary between 10 cm and 100 cm. The average slip amplitude ranged from 28 and 56 cm. These values are not consistent with Wells and Copersmith. These limits are arrived at by analysis of inversion results for slip distribution (Hartzell or Wald, many references), and results from Wells and Coppersmith (1994).

Roughness: of rupture is the percentage of the rupture surface for which we applied randomness to the rise time so that we could simulate roughness. The percentage is randomly selected to be 0, 10, 20, 33, or 50%. This percentage of elements has rise time randomly shortened to between 0.1 and 0.9 times the original value. The difference in rise time is applied as a delay to rupture initiation so that the rupture reaches the full value at the original time. Areas of roughness have corresponding high stress drop. Roughness for a particular element is created by shortening its rise time by a percentage between .1 and .9. The percentage is randomly chosen separately for each element with the random FORTRAN function. Roughness is implemented by and delaying an element's rupture time so that it finishes slip (rise time) at the same time as neighboring elements. This models the effect of an element rupturing later than neighboring elements, and having higher stress drop; i.e. the Schultz model of contact asperities. Asperities and background elements both have the same percentage of elements with roughness.

Asperities: are circular in shape and have an area that is between 10% and 40% of the total fault area. The number of asperities is randomly chosen to be between 0 and 7. So, although the number of asperities is roughly equal for any size fault, their relative size scales with the fault dimensions. This replicates observation with inversion studies, and suggests that smaller asperities are not significant to ground motion of larger earthquakes. Asperities have slip distribution defined by the Kostrov rupture with healing.

Rise Time: Rise time varies at each point on the fault and is a dependent variable. Rupture initiates at the arrival time of the rupture front, and continues until the shortest time for the rupture front to reach a fault edge and for a healing phase to travel back to the point at the

healing velocity. Healing is derived from dynamic rupture models (Das and Kostrov, 1990, and many others).

Rupture Velocity is allowed to vary from 0.75 to 1.0 times the shear wave velocity as derived from dynamic rupture modeling (Das and Kostrov, 1990, and many others)

Healing velocity is the percentage of the rupture velocity for the healing velocity. If the healing velocity is greater than the rupture velocity, it will shortly overtake the rupture front, and thus, no rise time will develop. We randomly varied healing velocity to between 0.8 and 1.0 times the rupture velocity, which is about between the Raleigh wave velocity and the shear wave velocity, as observed in dynamic rupture modeling.

Stress drop is a dependent variable derived from the Kostrov slip function. In this derivation, stress drop is that which results in a strain discontinuity and a displacement on the fault, and results in seismic radiation. It, then, is equivalent to the Orowan stress drop (Orowan, 1960). In our kinematic models, stress drop is allowed to vary due to four effects modeled in rupture. First, the overall average stress drop is directly dependent upon the moment and size of the rupture area, Second, “fault roughness” (described above results in small areas of relative high stress drop, Third, asperities are allowed to have a different stress drop than surrounding portions of the fault rupture; and fourth, stress drop is constrained to diminish near the surface of the earth at the rate of 10 + 0.75 times the confining pressure due to the lithostatic load (300 bars at 1.7 km depth). The minimum of this and the full rupture stress drop is used. Stress drop for the main event ranges from 3 to 40 bars, while the asperities range from 10 to 100 bars.

Rigidity varies with the shear wave velocity over all depths except it diminishes at the same rate as the stress drop near the surface. Rigidity is estimated by multiplying the shear wave velocity value by 1011. The diminishing of stress drop and rigidity near the surface has two effects. First, reducing the rigidity results in very little moment contribution for rupture near the surface. Second, the commensurate diminishing of stress drop and rigidity result in significant displacements (although not significantly seismogenic) at the surface.

Wossner et. al (2002) studied the effects of source parameter changes on acceleration time series and Flourier amplitude spectra using the program EMPSYN discussed here. They found that hypocenter location greatly affects near source satiations due to a directivity effect; different fault plane geometries significantly effects rise time distribution, and thus amplitude and frequency content of signal; and, variations in rupture and healing velocities can cause up to a

factor of five variation in amplitudes of time series. Obviously when these parameters are varied, they combine to give a distribution of ground motion amplitudes.

Error Analysis

We assume the following: the scenarios are all of equal probability, the hazard to the site is monotonic with response spectra, and the scenarios were randomly selected within the bounds of possible rupture parameters. Values for spectra discussed here are the average of the log of the two horizontal components. In the terminology of Abrahamson et al. (1990) our prediction uncertainty has three elements: (1) parametric uncertainty, which arises from uncertainty as to which scenario will occur, and (2) modeling errors caused by not modeling the actual rupture process correctly, and (3) and random errors caused by factors such as uncertainties in source parameter estimates for empirical Green's functions, errors caused by the interpolation of source events along the fault surface, and uncertainties in estimates of the log-normal mean and standard deviation of the distribution of the one hundred scenarios.

The hazard is defined by the AAR of the synthesized ground motions. The estimation of the median (log-normal mean) hazard is:

$$\hat{H}_j = \frac{1}{N}\sum_{i=1}^{N} \log(R_{ji}) \tag{7}$$

where, R_j is the absolute acceleration response. The index i ranges over the number of scenarios N, while j is the increments over 46 periods, from 0.05 sec to 1.0 sec, in which the AAR has been evaluated. The estimation of the 84 percentile (i.e. the average plus one standard deviation) is the combined effect of the prediction errors:

$$H_j^{\square} = \hat{H}_j + [\square_{pj}^2 + \square_m^2 + \square_e^2 + \square_r^2]^{1/2} \tag{8}$$

where: σ_p^2 is the variance of the distribution of the log(*AAR*) for N scenarios and is calculating for each of 46 periods; it has an average value of 0.098. It is an estimation of the uncertainty due to not knowing in advance which earthquake scenario is likely to occur; σ_m^2 accounts for modeling errors when the exact scenario is known, but not modeled correctly, and for random errors due to interpolation of empirical Green's functions. This error is unknown for this study, but is assumed to be equal to the standard deviation obtained by Jarpe and Kasameyer (1996), which is 0.0795; σ_r^2 is the variance of the computation of both the lognormal mean and the standard deviation, and it has a value of 0.0011 (Hutchings et al., 2002).

The variance due to random errors in source parameters (moment and source corner frequency)σ_e^2 greatly affects the synthesized seismograms with the approach used in this study. In equation (1) moment linearly-inversely scales the amplitude of synthesized seismograms, and the corner frequency used in the deconvolution of the Brune source from empirical Green's functions significantly effects the high frequency content of the synthesized seismograms. Moment is a difficult parameter to calculate. The scaling for moment in equation 2 is dependent upon seismic velocity is to the 4th power (density is determined from the P-wave velocity). A difference of 20% in velocity, for example, results in a change in moment value of about a factor of 2. Pavic et al (2000) identified the estimation of the moment of the empirical Green's functions as the most sensitive parameter for a synthesis approach essentially the same as EMPSYN. Wossner et al (2002) used the program EMPSYN and repeatedly calculated 24 source models using either one or several EGFs, and found a systematic bias if only one EGF was used, and that it is likely a result of in accurate moment calculations. They concluded that using several EFGs averaged out the uncertainties. Dan (1990) estimated the uncertainty in synthesized seismograms due to using only one EGF. He found that a 40 to 80% variation was reduced to 20% variation when 17 aftershocks were used in the synthesis instead of one. Gok et al (2003) estimated moment and source corner frequency of about 600 aftershocks of the 1999 Anatolian earthquakes with fifty stations using the program NetMoment (discussed above). They compared results of 10 events with those obtained from full S-waveform moment tensor inversion and found that moment estimates from NetMoment are with 10% agreement. Further, Gok et al (2004) used an f-test to find the range of source corner frequencies within 95% confidence and found NetMoment corner frequency's uncertainties of about 25% on average. Finally, they

compared corner frequencies of 10 events to those obtained with the parameter-less approach based upon coda-analysis of Mayeda and Gok (2004) and found an overlap of calculations. We calculated the standard deviation of a log10 normal distribution of the moment calculation for individual stations compared to the joint inversion result to be a factor of 1.3. From this we conclude that the error due to epistemic uncertainty in calculation moment to be 0.14 on a log scale. The average standard deviation of the hazard over all frequencies is a factor of 2.8.

Strong Ground Motion Prediction

One purpose of this paper is to predict the range of ground-motion that may occur from a particular magnitude earthquake within a source zone. We test this with the 1999 Athens earthquake. Considering the range of hypocenters for the 1999 earthquake, it likely occurred in the southeast corner of the larger area for magnitude 6 (Figure 2 and Table 2). Further, Papadimitriou et al (2000) identify a stopping phase and interpret Aegaleo Mountain acting as barrier to the main rupture, which initiated in the western part of the activated fault. Tselentis and Zahradnik, (2000) discuss a fault surface determined by the distribution of aftershocks occurring during an 11-day period at depths 3.5 to 15.5km, which coincides with the fault plane computed by the USGS. The absence of aftershocks in an 8x10 km area is interpreted as the area ruptured by the main event. EGFs waveform modeling by the same researchers allows for a larger area ruptured by the main event. In addition interferograms (Kontoes et al, 2000) present a deformed area of 20 km E-W by 10 km N-S with no fringes beyond the Aegaleo Mountain but with fringes extending to the east, north of Aegaleo Mountain. With these studies we confine the volume for the likely extent of rupture of the 1999 earthquake to be between 38.00^{o} and 38.14^{o} N, 23.53^{o} and 23.67^{o}E, and 0.0 to 20.0 Km in depth. This is a 12.3 x 15.3 x 20.0 Km volume that contains the entire rupture of the scenario events. We found that 63 models of the larger set of 500 (discussed below) fell within this volume, and there are used to test our prediction hypothesis.

We calculate the median (log-normal mean) and plus one standard deviation (STD) values of linear ground motion at sites ATHA, DMKA, FIXA, THVC, SGMA, and SPLA; and compare these to recorded values. The one STD values also include error for uncertainties in the methodology as discussed above. These are the only stations that recorded the main event and aftershocks at distinctly different sites. Stations SGMB and SPLB also recorded the main event and aftershocks, but they were to closely located to SGMA and SPLA to add to the test.

Figure 6 shows the Fourier amplitude spectra for each scenario, (dotted line), the plus and minus STD values of the prediction (thick dashed lines), and actual Fourier amplitude spectra recorded (thick solid line). Figure 7 shows the same plots for the absolute acceleration response (AAR). Both the Fourier amplitude spectra and AAR are at or below the one STD values as one might expect for the source volume studied. However, the recorded data is at the high end of the synthesized suite of spectra. Considering that the one STD values represent the 67% level, the actual records may not fall within the plus and minus one STD values. The fit near one standard deviation values may indicate that the actual earthquakes was an unusual event, the syntheses methodology is systemically bias to low values, the event modeled was actually larger than Mw = 6.0 assumed, or several other hypotheses. We conclude that first, the shapes of the spectra in general match the shapes of the observed spectra; that with the uncertainties in the epistemic and aleatory uncertainties assumed, the observed spectra fall within or very close to the one standard deviation values; and that we "pass" the prediction test. It will take several validation exercises similar to this one to determine whether the methodology has problems, such as a systemic bias. Including the previous validation tests discussed below, this is not yet evident.

Synthesized Strong Ground Motion

Another goal of the paper was to identify the most likely rupture scenario of what actually occurred during the 1999 Athens earthquake. We calculate the goodness of fit between observed and synthesized records by the method developed by Anderson (2003) to identify the best rupture models. Anderson suggests calculating the fit of Arias duration, energy duration, Arias intensity, energy integral, peak acceleration, peak velocity, peak displacement, absolute acceleration response, Fourier spectra, and cross-correlation. Arias intensity and energy integral are proportional to the integral of the acceleration and velocity squared, respectively. The Arias and energy durations are defined as these integrals normalized by their maximum value, and the goodness of fit is determined by one minus the maximum of the difference between the observed and calculated normalized integrals. Each estimate is given a value of 0 to 10, so that the final score is between 0 and 100, with the latter being a perfect fit. Anderson finds that 40 to 60 represents a fair fit, 60 to 80 a good fit, and 80 to 100 an excellent fit. All estimates for goodness of fit were averaged over their values at frequency bands 1-2, 2-5, 5-10, 10-20, and 1-20 Hz as suggested by Anderson (person communication); except Fourier and absolute acceleration response, which are calculated for each frequency 1 - 20 Hz only and averaged. We averaged the

values obtained from three components, and further averaged the values obtained at all six sites to get a final score that represents how well a rupture model generates the observed accelerograms.

Values for the 63 models ranged from 20 to 67. We found three models that had the best rating of fits to observed seismograms (models M204, M250 and M348, with ratings of 67, 61 and 64, respectively). The three models are shown in Figure 8. They all had very similar rupture models; they occurred in the vicinity of 38.05o N 23.60o W with center of rupture near 12 km, and near unilateral rupture towards Athens. Strikes range from N107oE to N115oE, dips range from 39o to 48o, rupture velocity range from 0.92 to 0.99 times Vs, and healing velocity ranged from .89 to .95 times Vr. Although the rupture models are very similar, the fit to observed seismograms is better at some stations than at others. However, all three models matched the shape of the spectra well at most stations, and those from model M204 generated the best seismograms by the Anderson method, and by eye. Figure 9 shows the fit to recorded seismograms for this model. The fit to seismograms suggest that for engineering purposes, this methodology can provide realistic ground motion in advance of an earthquake that includes what will actually happen.

From Figure 9, it is apparent that the shape of the spectra and character of the time series are matched well at each station (a couple of obvious exceptions). In particular, the basic waveforms and durations of the time series, and the shape of the Fourier amplitude and acceleration response spectra are matched well. Notice that the spectral shapes and character of the seismograms are considerably different at each site. The site-specific character of these factors is controlled by the empirical Green's functions and the geometric relationship to the source rupture. It is interesting to compare Figure 5 with Figure 9; Figure 5 shows the basic character of the empirical Green's function at each site that includes only the propagation path and site effects, and Figure 9 shows the resulting seismograms when they are convolved with the rupture model of the main event. The basic character of the high frequency spectral shapes is the same.

Our basic assumption is that if accelerograms give a good fit to observed records, then the rupture model is near what actually happened. Since the fit is to low and high frequency, and acceleration, velocity, and displacement; and since the "true" Green's functions are used, this seems a fair assumption. One can image that iterating around the rupture parameters of models M204, M250, and M348, one could find an even better fitting model. We ran HAZARD for 25

models in the vicinity of the parameters of these models, but did not find a better fitting set of synthesized seismograms on average. We also ran 20 models with small variations around model M204. We kept the fault geometry and hypocenter the same and only varied the rupture and healing velocity, roughness, and asperities. This did not result in any significant improvement. We conclude from our basic assumption that the actual Athens earthquake had a rupture similar to those of models M204, M250, and M348. Also, our "best" fitting model is near the limit of what we can achieve with modeling exact rupture and fitting seismograms with this methodology.

Extrapolation of Ground Motion

Another goal of this paper was to model ground motion in areas where the main earthquake was not recorded. We have used the rupture scenario ATH204 to model accelerograms at stations COUR, PEFK, PSAR, MAGO, ZOFR, and NEOK (STEF had a bad horizontal component). The reader is referred to Ioannidou et al. (2001), where the geology and site response of these sites and other sites referred to in this paper are extensively examined. Figure 10 shows the synthesized seismograms at these stations. In general station MAGO had significant accelerations in the 0.2 g range, stations COUR, ZOFR, and NEOK had significant accelerations in the 0.3 to 0.4 g range, and stations PEFK and PSAR had significant accelerations in the 0.4 to 0.8 g range. Stations ZOFR and COUR are in the intensity VIII zone, and stations PEFK, PSAR, MAGO, and NEOK had intensities in the VII zone (Figure 2). Stations SPLA, which recorded the main event (Figure 9), are also in the intensity VII zone, and it had accelerations in the 0.3 g range. All these sites, except MAGO, had accelerations greater than the other actual recorded strong motions, which ranged form 0.04 to 0.2 g. From Ioannidou et al (2001), station MAGO showed a de-amplification of site response relative to the other sites, PSAR, ZOFR, COUR, showed amplifications up to a factor of 6 at some frequencies. NEOK and SPLA were reference sites in the Ioannidou et al. study, and therefore were considered natural in amplification. Station PEFK was not studied by Ioannidou et al. These sites are located in the up dip direction of the presumed fault (Figure 8). The sites where strong motion was actually recorded were located more of an off angle from the fault (except SPLA). Model 204 had a near unilateral rupture in the up dip direction of fault rupture. It is concluded that the observed high intensity values were due to a combination of site response and directivity effect of the fault rupture. Without site response, it is expected that accelerations would have been in the 0.3 g

range as observed for NEOK and SPLA, still greater in general that the actual recorded sites, and without de-amplification MAGO would also have had accelerations in the 0.3 g range.

Probabilistic Seismic Hazard Study for Athens

We synthesized 500 earthquakes distributed throughout a source volume likely to have Mw=6.0 earthquakes near Athens (Figure 2) in order to perform a limited probabilistic hazard study. We narrated 500 synthesized three- compound accelerograms for frequencies 1.0 to 20.0 Hz at stations (ATHA, DMKA, FIXA, THVC, SPLA, and SGMA). We assumed an average return period of 1000 years for this magnitude earthquake in the particular source zone, thereby having simulated a catalog of ground motion for a period of 500,000 years. The distribution of traditional ground motion parameters of peak acceleration or spectral ordinates can be obtained from these synthesized ground motions, from which we develop hazard curves in the form of the annual probability of exceedance. In future hazard studies, these types of ground motions might be used directly into building response models to calculate risk.

The larger source zone volume is interpreted from the neotectonics of greater Attica area. Though Athens has been affected by stronger more distant events. Neotectonic faults capable of an event of the moment of this study are the largest considered likely to occur in the vicinity of Athens metropolitan area. This consists of a complex post-alpine structure, which is characterized by complicated kinematic and dynamic evolution and involves major fault blocks with different rotational axes trending NE-SW and E-W. This structure consists primarily of the tectonic graben of Thriassion plain and the complex neotectonic graben of West Athens basin; the mountains of Parnitha and Aegaleo belonging to the Mesozoic non-metamorphic Eastern Greece unit; and the Pendeli and Ymittos mountains belonging to the Mesozoic metamorphic unit (Figure 3). The tectonic contact of these units is interpreted to be in the NE-SW direction with its location coinciding with the Kifissos River (Mariolakos and Foundoulis, 2000); this roughly coincides with the Miocene thrust feature shown in Figure 3. We thus confine the rupture area of any likely M = 6.0 earthquake to be confined to lie between 38o 00' and 38o 15' N, and between 23o 25' and 23o 40' E so that the morphological features of the Aegaleo Mountain to the southeast and the Kifissos River to the northeast, define the extension of the proposed rupture area to the East. Additionally, the proposed rupture area extends N-S to include mostly the Parnitha Mountain area, and is defined south by the Thriassion fault zone and north

by the change in the geological border between the Neopalaeozoic-Triassic-Jurassic Metamorphic Rocks Unit and Neogene and Quaternary Unit (Figure 3).

Figure 11 shows the plus- and minus-standard deviation of the distribution of Fourier amplitude spectra for the 500 models. Individual spectra for only 100 of the 500 models are shown. The standard deviation represents the distribution of ground motion that could possible effect the site. It is instructive to compare Figure 6 with Figure 11. Figure 11 shows a broader distribution and generally lower values, except at station THVC, where overall values increased. These effects are due to a greater distribution of distances, more sources farther away (or closer for THVC), and due to combinations of rupture that caused extreme ground motions. The effect of extreme ground motions is evident in spectra for stations SGMA, SPLA, ATHA, DMKA, and FIXA, where no sources closer than were already used form Figure 6 are added, but several (out of only 100) significantly higher amplitude ground motions are present in Figure 11.

Figure 12 shows bar graphs of AAR at 0.5 sec at the six sites. This represents the complete history of this ordinate value for 500,000 years from magnitude 6.0 earthquakes (based on our assumptions). Presumably, this is a long enough period of history that if another 500,000 years passed, no different distribution of ground motion would occur. These values then represent all values that could ever affect the site, and thus the complete hazard. Shown on Figure 12 are vertical lines along the abscissa axes; these are values where only one vent contributed the bar graph. These, tend to be outliers from the main distribution. These represent "extreme" events. Their values range form 2 to 5 times the standard deviation. Interestingly, a scenario that produces an extreme event at one station may not do so at other stations. Figure 12 also shows the annual probability of exceedance form the 0.5 sec AAR at the six sites. This is the PSHA for this ordinate value from magnitude 6.0 earthquakes. Also, shown is the ground motion that actually occurred. By our PSHA the 1999 earthquake that occurred was a 10^{-5} event.

Conclusions

We tested a methodology to predict the range of ground-motion hazard for a fixed magnitude earthquake along a specific fault or within a specific source volume. We fixed the moment to be that of the 1999 Athens earthquake and synthesized 100 rupture scenarios in a source volume estimated to be the likely location for an earthquake of this size near Athens. In our test we found that the plus one standard deviation of engineering parameters predicted was generally about equal to what actually occurred. Considering that the one STD values represent

the 67% level, the likelihood of an earthquake falling outside the plus and minus STD values is about 30%. This suggests that the likelihood of having an earthquake such as the 1999 Athens earthquake that is above the one STD value was about 15%. This is because for the source volume considered. Most of the rupture models that gave fits to actual seismograms occurred in the vicinity rupture models; they occurred in the vicinity of 38.05^{o} N 23.60^{o} W with center of rupture near 12 km, and near unilateral rupture towards the northeast of Athens. Strikes range from N107^{o}E to N115^{o}E, dips ranges from 39^{o} to 48^{o}, rupture velocity range from 0.92 to 0.99 times Vs, with a rupture directivity partially towards Athens and directivity in the direction for the highest damage areas.

We also synthesized strong motion records in high damage areas for which strong motion records do not exist. Peak accelerations range from about 0.1 g at station MAGO to 0.2 g at stations COUR, ZOFR, and PSAR. Stations COUR, ZOFR and PEFK are near the highest intensity values from this earthquake (Figure 2) and have relatively high peak accelerations. Another application of the methodology demonstrated here is to extend the work described here to a full range of moments and all possible sources and use the results to conduct a full synthetic probabilistic hazard study.

The slip distribution of our best models agrees well with those of previous studies. Tselentis and Zahradnik (2000) modeled the rupture with empirical Green's functions, using Irikura's synthesis approach, at one station over 200 km distant and had a similar fault size, orientation and location as this study. Roumelioti et al (2003) also modeled the Athens earthquake with an empirical Green's function method, different from this paper or Irikura's method, at nine regional stations greater than 200 km distant and found a slip distribution and strong unilateral rupture similar to this study.

Synthesized seismograms are very complicated and site specific, and each spectra has a shape that is due to the site-specific effects, and the source spectra is fairly simple. This suggests that a lot of source models have too much complexity due to having too simple of Green's functions. We used aftershocks (M<4.0) that are larger than the criteria for having impulsive point sources and were distributed throughout the area. We deonvolved out the finite source effects of the empirical Green's functions to generate impulsive point shear source empirical Green's functions. Using events that are not necessarily along the fault to be modeled is assumed to result in an average propagation path effect and site specific site response, and this assumption appears to be validated

because of the match to observed seismsograms. Also, the fit to seismograms suggest that for engineering purposes, this methodology can provide realistic ground motion in advance of an earthquake that includes what will actually happen. We developed constraints on rupture parameters based on prior knowledge of earthquake rupture processes and sources in the region; ran a sufficient number of scenario earthquakes to span the full variability of ground motion possible; found that our distribution of synthesized ground motions span what actually occurred and their distribution is realistically narrow; determined that one of our source models generates records that match observed time histories well; found that certain combinations of rupture parameters produced "extreme" ground motions at some stations; and, identified that the "best fitting" rupture models occurred in the vicinity of 38.05^{o} N 23.60^{o} W with center of rupture near 12 km, and near unilateral rupture towards the areas of high damage, and this is consistent with independent investigations. We also synthesized strong motion records in high damage areas for which records from the earthquake were not recorded, and found relatively high ground motion that would explain the higher level of damage in this area.

References

Aki, K. (1969). Analysis of the seismic coda of local earthquakes as scattered waves, J. Geophys. Res. 74, 615-631.

Aki, K. and P. G. Richards (1980). Quantitative seismology, Theory and Methods, Volumes I and II, W. H. Freeman and Company, San Francisco, CA.

Anagnostopoulosa, S. A., Theodoulidis N. P., Lekids, B. A. and Margaris, B. N. (1986). Kalamata earthquake Sep. 13, 1986. Research Rep. 86-06. Institute of Engineering Seismology and Earthquake Engineering (ITSAK), Thessaloniki.

Anderson, John G. (2003) A Criterion for Evaluating Goodness of Fit of Accelerograms. 13th World Conference, in press.

Anderson, John G. and James Brune (1999) Probabilistic seismic hazard analysis without the ergodic assumption. Seism. Res. Lett., 71, No.1, pp. 19-28.

Anderson, J. G. and S. Hough (1984). A model for the shape of the Fourier amplitude spectra of accelerograms at high frequencies, Bull. Seis. Soc. Am. 74, 1969-1994.

Andrews, D. J. (1986). Objective determination of source parameters and similarity of earthquakes of different size, Earthquake Source Mechanics, American Geophysical Union, Washington, D.C., 259-267.

Attiko Metro (1999). Internal Geotechnical Report, personnel communication with Ioannis Kalogeras.

Baise, L.G. and S.D. Glaser (2000). Consistency of ground-motion estimates made using system identification, Bull. Seis. Soc. Am. 90, 993-1009.

Baise, Laurie, Lawrence Hutchings, and Steven Glaser (2002). Analysis of site response at Yerba Buena Island, San Francisco Bay, California from weak motion recordings, Special Issue on Site Response, Bollettino Di Geofisica teorica ed applicata, this issue.

Basili, M. and Brady, G. (1978). Low frequency filtering and the selection of limits for accelerogram corrections. Proc. of VI European Conference on Earthquake Engineering, Sep 18-22, Dubrovnik, Yugoslavia, 251-258.

Blakeslee, S. and P. Malin (1991). High-frequency site effects at two Parkfield downhole and surface stations. Bull. Seis. Soc. Am. 81, 332-345.

Boatwright, J. L (1981) Quasi-dynamic models of simple earthquake: an application to an aftershock of the 1975 Oroville, California earthquake. Bull. Seis. Soc. Am. 71, 69-94.

Bommer, Julian J., Norman A. Abrahamson, Fleur O. Strasser, Alain Pecker, Pierre-Yves Bard, Hilmar Bungum, Fabrice Cotton, Donat Fah, Fabio Sabetta, Frank Scherbaum, and Jost Studer (2004) The Challenge of Defining Upper Bounds on Earthquake Ground Motion. Seis. Res. Lett., 75, No. 1.

Bonilla, Luis Fabian, Jamison H. Steidl, Grant T. Lindley, Alexei G. Tumarkin, and Ralph J. Archuleta (1997). Site amplification in the San Fernando valley, CA: variability of the site effect estimation using the S-wave coda, and H/V methods. Bull. Seis. Soc. Am. 87, 710-730.

Borcherdt, R. D. (1970). Effects of local geology on ground motion near San Francisco Bay. Bull. Seis. Soc. Am. 60, 29-61.

Bouckovalas, G. D., Kouretzis, G. and Kalogeras, I.S. Site-specific analysis of strong motion data from the September 7, 1999 Athens, Greece earthquake. (Natural Hazards, in press).

Brune, J. N. (1971). Tectonic stress and the spectra of seismic shear waves from earthquakes, J. Geophys. Res. 75, 4997-5010 (Correction, J. Geophys. Res. 76(20), 5002, 1972).

Caceci, M. S. and W. P. Cacheris (1984). Fitting curves to data, Byte Magazine, May, 340-360.

Carydis, P. G., Drakopoulos, J. and Taflambas, J. (1984). Evaluation of the Corinth strong motion records of February 24 and 25, 1981. Proc. of EAEE, Athens.

Carydis, P. G., Drakopoulos, J., Kalogeras, J., Mouzakis, H., Taflambas, J. and Vougiouka, N. (1989). Analysis of the Kalamata, Greece, strong motion records and correlation with the observed damages. Proc. of XXI General Assembly of E.S.C., 23-27 Aug. 1988, Sofia, Bulgaria, 344-355.

Cohee, B. P. ,P. G. Sommerville, and N. A. Abrahamson (1991) Simulated Ground Motions for Hypothesized Mw= 8 Subduction Earthquakes in Washington and Oregon. Bull. Seism. Soc. Am. 81, 28-56.

Cornell, C. A. (1968). "Engineering Seismic Risk Analysis", Bull. Seism. Soc. Am. 58, 1583-1606.

Dan, K., T. Watanabe, T. Tanaka, and R. Sato (1990) Stability of earthquake ground motion synthesized by using different small-event records as empirical Green's functions. Bul. Seis. Soc. Am. 80, 1433-1455.

Edafomechaniki, Ltd. (1998). Geotechnical study of the Thiva area. Ministry of Development, General Secretariat of Research and Technology, Auto-Seismo-Geotech, Vol B, Report 4.1.

EERI (1999). The Athens, Greece earthquake of September 7, 1999. Special earthquake report - Learning from Earthquakes. November 1999.
http://www.eeri.org/earthquakes/Reconn/Greece1099/Greece1099.html.

Field, E. H. and K. H. Jacob (1993). The theoretical response of sedimentary layers to ambient seismic noise. Geophysical Resear4ch Letters. 20 (24), 2925-2928.

Foxall, William, Lawrence Hutchings, and Paul Kasameyer (1994) Lithological and rheological constraints on fault rupture scenarios for ground motion hazard prediction. IUTM Symposium on Mechanics Problems in Geodynamics, Sept. 5-9, 1994, Beijing, China; UCRL-JC 116437 Lawrence Livermore National Laboratory, pp 27. accepted to Bul. Seis. Soc. Am, 1996.

Frankel, A. and L. Wennerberg (1989). Microearthquake spectra from the Anza, California, seismic network: site response and source scaling, Bull. Seis. Soc. Am. 79, 581-609.

Geomechaniki Ltd. (1999) Geotechnical report for the Planetarium Building at Evgenidis Foundation. pp. 10.

Glaser, S. D. (1995). System identification and its application to Estimating Soil Properties. Journal of Geotechnical Engineering, 553-560.

Guatteri, Mariagiovanna P., Martin Mai, Gregory C. Beroza, and John Boatwright (2003) Strong Ground-motion Prediction from Stochastic-Dynamic Source Models. Bull. Seis. Soc. Am. 93, 301-313.

Hanks, T.C. and H. Kanamori (1979) A moment magnitude scale. J. Geophys. Res. 84, 2348-2350.

Hartzell, S.H. (1982) Simulation of ground accelerations for May 1980 Mammoth Lakes, California, earthquakes, Bull. Seis. Soc. Am. 72, 2381-2387.

Hartzell, S.H. (1992) Site response estimation from earthquake data. Bull. Seis. Soc. Am. 82, 2308-2327.

Hartzell, Stephen, Stephen Harmsen, Arthur Frankel. and Shawn Larsen (1999) Calculation of Broadband Time Histories of Ground Motion: Comparison of Methods and Validation using Strong-Ground Motion from the 1994 Northridge Earthquake. Bull. Seis. Am. 89, 1484-1504.

Hashida, T. Stavrakakis, G. and Shimazaki, K. (1988). Three-dimensional seismic attenuation structure beneath the Aegean region and its tectonic implication. Tectonophysics, 145, 43-54.

Hatzidimitriou, P., Papazachos, C., Kiratzi, A. and Theodoulidis, N. (1993). Estimation of attenuation structure and local earthquake magnitude based on acceleration records in Greece. Tectonophysics, 217, 243-254.

Heaton, T. H. (1982). The 1971 San Fernando earthquake: a double event? Bull. Seism. Soc. Am., 72, part A, 2037_2063.

Hough, S. E., J. G. Anderson, J. Brune, F. Vernon III, J. Berger, J. Fletcher, L. Harr, T. Hanks, and L Barker (1988)Attenuation near Anza, California, Bull. Seis. Soc. Am. 78, 672-691.

Hudson, D. E. (1979). Reading and interpreting strong motion accelerograms. EERI, Pasadena, California, 1-112.

Hudson, D. E. and Brady, A. G. (1971). Strong motion earthquake accelerograms - Digitized & plotted data. Vol. IIA. EERL, 71-50, California Institute of Technology, Pasadena, California.

Hutchings, L. (1988). Modeling strong earthquake ground motion with an earthquake simulation program EMPSYN that utilizes empirical Green's functions, Lawrence Livermore National Laboratory, Livermore, CA, UCRL-ID-105890, p. 122.

Hutchings, L. (1991). ÒPredictionÓ of strong ground motion for the 1989 Loma Prieta earthquake using empirical Green's functions, Bul. Seis. Soc. Am. 81, 88_121.

Hutchings, L. (1994) Kinematic Earthquake Models and Synthesized Ground Motion Using Empirical Green's Functions. Bul. Seis. Soc. Am. 84, pp. 1028-1050.

Hutchings, Lawrence, P.W. Kasameyer and W. Foxall (2003) LLNL, Hazard Mitigation Center Ground Motion Prediction Methodology. Lawrence Livermore National Laboratory, UCRL-ID 135697.

Hutchings, Lawrence (2002) Program NetMoment, a Simultaneous Inversion for Moment, Source Corner Frequency, and Site Specific t*. Lawrence Livermore National Laboratory, UCRL-ID 135693.

Hutchings, L. and F. Wu (1990). Empirical Green's functions from small earthquakesÑA waveform study of locally recorded aftershocks of the San Fernando earthquake, J. Geophys. Res. 95, 1187_1214.

Hutchings, L.J., S.P Jarpe, P.W. Kasameyer and W. Foxall (1996) Synthetic Strong Ground Motions for Engineering Design Utilizing Empirical Green's Functions. proceedings Fourth Caltrans Seismic Research Workshop, pp. 24; Eleventh World Conference of Earthquake Engineering, Acapulco, June 23-28, 1996 (CDROM Elsevvier); LLNL, UCRL-JC-123762.

Hutchings, Lawrence, Eleni Ioannidou, Steven Jarpe, and Giorgis N. Stavrakakis (1997) Strong Ground Motion synthesis for a M=7.2 Earthquake in the Gulf of Corinth, Greece using Empirical Green's Functions. UCRL-JC-129394 Lawrence Livermore National Laboratory.

Hutchings, Lawrence, Steven Jarpe, Paul Kasameyer (1998) Validation of a Ground Motion Synthesis and Prediction Methodology for the 1988,M=6.0, Saguenay Earthquake.UCRL-JC-129395 Lawrence Livermore National Laboratory.

Idriss, I. M. (1990). Response of Soft Soils during Earthquakes. H. Bolton Seed Volume 2 Memorial Symposium Proceedings, ed. J. Michael Duncan.

Ioannidou, Eleni, Nicholas Voulgaris, Ioannis Kalogeras, Lawrence Hutchings, and George Stavrakakis(2001). Analysis of Site Response in the Athens Area from the 7 September 1999, Mw=5.9 Athens Earthquake and Aftershock Recordings, and Intensity Observations. Special Issue on Site Response, Bollettino Di Geofisica teorica ed applicata, December 2001.

Jarpe, S.J. and P. K. Kasameyer (1996) Validation of a Methodology for Predicting Broadband Strong Motion Time Histories using Kinematic Rupture Models and Empirical Green's Functions. Bul. Seis. Soc. Am. 86, pp1116-1129.

Kalogeras, I. S. and Stavrakakis, G. N. (1999). Processing of the strong motion data from the September 7th, 1999 Athens earthquake. National Observatory of Athens, Geodynamic Institute, Publ. No 10 (CD-ROM).

Katsikatsos, G., G. Migiros, M. Triandaphyllis and A. Mettos (1986). Geological Structure of Internal Hellenides. Geological and Geophysical Research Special Issue IGME, pp. 191-212, Athens.

Kouskouna,V., Makropoulos, K., Raftopoulos, D., Malakatas, N., Albini, P., Stucchi, M. and Rubbia, G. (2000). The September 7, 1999, Parnitha earthquake: Macroseismic observations Abstract in EGU, Sept. 2000, Lisbon, Portugal.

Lachet, C. and P.-Y. Bard (1994) Numerical and Theoretical Investigations on the possibilities of NakamuraÕs Technique. Journal of Physics of the Earth, 42, 377-397.

Lama, R. D. and V. S. Vutukuri (1978). Handbook on Mechanical Properties of Rocks, V II, R.D. Trans Tech Publications, p. 245, pp. 481.

Lekidis, V., K. Pitilakis, V. Margaris, N. Theodoulidis and A. Moutsakis(1991). The Edessa earthquake of Dec. 21, 1991. Report 91-01, Institute of Engineering Seismology and Earthquake Engineering (ITSAK), 1-68.

Lekkas, E. (2001) The Athens earthquake (7 Sept. 1999): intensity distribution and controlling factors, Engineering Geology 59 (2001) 297-311.

Lermo, J. and Chavez-Garcia (1993). Site Effect Evaluation using Spectral Ratios with only one Station. Bull. Seism. Soc. Am. 83, 1574-1594.

Larsen, Shawn (1994) Adaptation of finite difference code to Meiko parallel computer.

Lindley, Grant T. and Ralph J. Archuleta (1992). Earthquake Parameters and the Frequency Dependence of Attenuation at Colinga, Mammoth Lakes, and the Santa Cruz Mountains, California. J. Geophys. Res. 97, No. B10, 14137- 14154.

Makropoulos, K., Drakopoulos, J. and Kouskoun, V. (1989). The earthquake sequence in Volos, Central Greece, April 30, 1985. Analysis of strong motion. IASPEI, (Abstracts), Istanbul, 1989.

Malagnini, Luca, Robert b. Herrmann, and Massimo Di Bona (2000) Ground-Motion Scaling in teh Apennines (Italy). Bull. Seis. Soc. Am. 90, 1062-1081.

Malin, P. E. (1980). A first-order scattering solution for modeling elastic waves codas. I. The acoustic case. Geophys. J. R. Astr. Soc. 63, 361-380.

Margaris, V. N. (1986). Digitizing errors and filters. Report 86-03, Institute of Engineering Seismology and Earthquake Engineering (ITSAK), 1-43.

Mariolakos, I. and I. Foundoulis (2000). The Athens Earthquake Sept. 7, 1999, the Neotectonic Regime of the Affected Area. Ann. Geol. des Pay Helleniques, Tom. XXXVIII, Fasc. B.

McCallen, D.B. and L.J. Hutchings (1996) Ground motion estimation and nonlinear seismic analysis. LLNL, UCRL-JC-121667. proceedings: 12th Conference on Analysis and Computation of the American Society of Civil Engineers, Chicago, Illinois, pp. 34-45.

Nakamura, Y. (1989). A Method for Dynamic Characteristics Estimation of Subsurface using Microtremors on the Ground Surface. Quart. Review of Rail. Trans Research Institute

National Research Council (1997). "Review of Recommendations for Probabilistic Seismic Hazard Analysis: Guidance on Uncertainty and Use of Experts", National Academy Press, Washington, D.C., 73 p.

Nelder, J. A. and R. Mead (1965). A simplex method for function minimization, Computer J., 7, 308.

Nigam, N.C. and Jennings, P.C. (1968). Calculation of response spectra from strong-motion earthquake records. Bull. Seism. Soc. Am. 58, 909-922.

Papadimitriou, P., G. Kassaras, N. Voulgaris, I. Kassaras, N. Delibasis, and K. Makropoulos (2000). The September 7, 1999 Athens Earthquake Sequence Recorded by the Cornet Network: Preliminary Results of Source Parameters Determination of the Mainshock. Ann. Geol. des Pay Helleniques, Tom. XXXVIII, Fasc. B.

Papadopoulos, G. A., G. Drakatos, D. Papanastassiou, I. Kalogeras, G. Stavrakakis (2000). Preliminary Results about the Catastrophic Earthquake of 7 September 1999 in Athens, Greece. Seis. Res. Let. 71, No. 3, pp.318-329.

Papageorgiou, A. S. and K. Aki (1983) A specific Barrier model for the Quantitative description of inhomogeneous faulting and the prediction of strong ground motion, I, description of the model, Bull. Seism. Soc. Am. 73, 693-722.

Papazachos C. (1992). Anisotropic radiation modeling of macroseismic intensities for estimation of the attenuation structure of the upper crust in Greece. Pageoph, 138, 445-469.

Pavic, Ronan, Martin G. Koller, Pierre-Yves Bard & Corinne Lacave-Lachet (2000) Ground Motion prediction with the empirical Green's function technique: an assessment of uncertainties and confidence level. Journal of Seismology 4: 59-77.

Press, William H., Brian P. Flannery, Saul A Teukalsky, and William T. Vetterling (1998). Numerical Recipes, Cambridge University Press.

Protonotarios I. (1999). Preliminary conclusions from the Sept. 9, 1999 Earthquake. Workshop on The Sept. 9, 1999 Athens Earthquake, November 2, 1999 Athens, Greece.

PWRC (1981).Public Works Research Center Internal Report, A geotechnical study for a municipal building at Ag. Ioannie Rentis, laboratory tests. pp. 2.

Rollins, K. M., M. D. Mchood, R. D. Hryciw, and M. Homolka (1994) Ground Response on Treasure Island. Strong Ground Motion. pp. A109-A121.

Roumelioti, D. Dreger, A. Kiratzi, and N. Theodoulidis (2003) Slip Distribution of the 7 September 1999 Athens Earthquake Inferred from Empirical Green's Function Study. Bul. Seis. Soc. Am. V. 93, pp 775-782.

Rosset, Ph., J-J Wagner, M. Garcia-Fernandez, M. J. Jimenez (1998) Strong Ground motion Simulation with Empirical Green's Functions; First Attempts in the Framework of the European Project SERGISAI. EC Environment Research Programme, Climatology and Natural Hazards (1994-1998).

Roumelioto, Z., D. Dreger, A. Kiratzi, and N. Theodoulidis (2003) Slip Distribution of the 7 September 1999 Athens Earthquake Inferred from Empirical Green's Function Study. Bull. Seism. Soc. Am. 93, 775-782.

Rudnicki, J. W., and L. B. Freund (1981). On energy radiation from seismic sources, Bull. Seism. Soc. Am. 71, 583-595.

Safak, E. (1997). Models and Methods to Characterize Site Amplification from a Pair of Records. Earthquake Spectra. 13(1), 97-129.

Safak, E. (2002). Site Response Estimation from Ground Motion Records. Special Issue on Site Response, Bollettino Di Geofisica teorica ed applicata, this issue.

Schnabel, P., Seed, H. B., and J. Lysmer (1972). SHAKE: A Computer Program for Earthquake Response Analysis of Horizontally Layered Sites. Report No. UCB/EERC-72/12, Earthquake Engineering Center, University of California, Berkeley.

Seed, R. B., S. E. Dickson, and I. M. Idriss (1991) Principal Geotechnical Aspects of the 1989 Loma Prieta Earthquake. Soils and Foundations, 31 (1), 1-26.

Seed, H.B., Murarka, R., Lysmer, J. and Idriss, I.M. (1976). Relationships of maximum acceleration, maximum velocity, distance from source, and local site conditions for moderately strong earthquakes. Bull. Seism. Soc. Am. 66, 1323-1342.

Shakal, A.F. and Ragsdale, J. (1984). Acceleration, velocity and displacement noise analysis for the CSMIR accelerogram digitization system. Proc. of VIII World Conference on Earthquake Engineering, San Francisko,1984, Vol. II, 111- 118.

Sibson, R. (1986), Rupture Interaction with Fault Jogs, in Earthquake Source Mechanics, in S. Das, J. Boatwright, and C. H. Scholz, Eds., Am. Geophys. Un. Monograph No. 37 (Washington, D.C.), pp. 157_167.

Somerville, Paul, Kojiro Irikura, Robert Graves, Sumio Sawada, David Wald, Norm Abrahamson, Yoshinori Iwasaki, Nancy Smith, and Akira Kowada (1999) Characterizatizing Crustal Earthquake Slip Models for the Prediction of Strong Ground Motion. Seis. Res. Lett., 70, No. 1, pp 59-80.

Spudich, P. and L. N. Frazier (1984) Use of ray theory to calculate high-frequency radiation from earthquake sources having spatially variable rupture velocity and stress drop. Bull. Seism. Soc. Am. 74, 2061-2082.

Stavrakakis, G. N., Kalogeras, I. S. and Drakopoulos, J. C. (1993). Preliminary analysis of Greek accelerograms recorded at stations of NOA's network: Time period 1973 - 1990. Proc. 2nd Congress Hellenic Geophys. Union, Florina, Greece, 5-7 May, 175-191.

Stavrakakis, G. (1999) The Athens Earthquake of September 7, 1999, *Newslettrer of the European Centre on Prevention and Forcasting of Eathquakes* 3, 26-29.

Steidl, Jamison H., Alexei G. Tumarkin, and Ralph J. Archuleta (1996) What is a reference site? Bul. Seis. Soc. Am. 83, pp. 1733-1748

Steidl, J. (1993). Variation of Site Response at the UCSB Dense Array of Portable Accelerometers. Earthquake Spectra, Vol 9 (2).

Trifunac, M. D. and Lee, V. W. (1973). Routine computer processing of strong-motion accelerograms. EERL, 73-03.

Trifunac, M. D. and Lee, V. W. (1979). Automatic digitalization and processing of strong-motion accelerograms. Part I. Univ. Southern California, Tech. rep. CE, 79-151.

Trifunac, M. D., Udwadia, F. E. and Bbrady, A. G. (1973). Analysis of errors in digitized strong-motion accelerograms. Bull. Seism. Soc. Am. 63, pp __.

Tsamis (1999). Study for the development and extension of the building of the Nuclear Technology and Radiation Protection Institute.Nuclear Center for Scientific Research "Demokritos".

Tse, S. T., and J. R. Rice (1986), Crustal Earthquake Instability in Relation to the Depth Variation of Frictional Slip Properties, J. Geophys. Res. 91, 9452_9472.

Tselentis, G-Akis and Jiri Zahradnik (1999). Aftershock Monitoring of the Athens Earthquake of 7 September 1999. Seis. Res. Let., 71, No. 3, pp 330-337.

Tumarkin, A. G. and R. J. Archuleta (1997). Recent Advances in Prediction and Processing of Strong Motions, Natural Hazards, 15, 199-215.

Tumarkin, A. G. (1998) Seismic Energy Radiation from Earthquake Source Models. Notes for a talk at the Seminar on Strong Motion Seismology at the Disaster Prevention Research Institute of the Kyoto University.

Voulgaris, N., I. Kassaras, P. Papadimitriou, and N. Delibasis (2000). Preliminary Results of the Athens September 7, 1999 Aftershock Sequence. Ann. Geol. des Pay Helleniques, Tom. XXXVIII, Fasc. B.

Wells, Donald L. and Kevin J. Coppersmith (1994) New Empirical Relationships among Magnitude, Rupture Length, Rupture Width, Rupture Area, and Surface Displacement. Bul. Seis. Soc. Am. 84, pp. 974-1002.

Wossner, J., M. Treml and F. Wenzel (2002) Simulation of Mw = 6.0 earthquakes in the Upper Rhinegraben using empirical Green functions. Geophys. J. Int, 151, 487-500.

Acknowledgments
We benefited from reviews by Prof. K. Pitilakis and Prof. J. Zahradnik. We also benefited from discussions with Paul Kasameyer and William Foxall. This project was partially funded by the National Observatory of Athens, Greece, which also contributed significant data and data processing. The University of Athens, Greece contributed significant computational facilities and data. This project was partially conducted at Lawrence Livermore National Laboratory, under the auspices of the U.S. Department of Energy by the University of California, under contract No. W-7405-Eng-48. It was partiallyfunded by Caltrans under contract #59A0238.

Table 1: Station Information

Station	Latitude	Longi-tude	Location	Orient. l, .t +90.0	No. EGF	Geol class
ATHA+	38.00°N	23.77°E	Neo Psihiko;3-s reinforced concrete (RC); -13m	N180°E	16	c
ATHB++	37.93°	23.70°	Neo Faliro; Planetarium,3-s RC	120°	4	c
COUR**	38.10°	23.65°	Fili, Soccer Stadium	0°	5	a
DEKL++	38.10°	23.78°	Dekelia, Air Base, 1-story	175°*+	4	c
DFNA+	37.95°	23.74°	Dafni; Metro station, -14m	155°*+	0	c
DMKA+	37.99°	23.82°	Ag.Paraskevi; Research center, 1-story RC	135°	4	b
FIXA+	37.96°	23.73°	Sygrou-Fix; Metro station, -15 m	140°	4	c
PEFK**	38.08°	23.62°	Thriassion plain, Ware House, 1-story	0°	6	c
PNTA+	38.00°	23.79°	Papagos; Metro station, -15m	135°	0	c
RFNA+	38.02°	23.99°	Private building, 1-s wood	250°*+	0	b
RNTA++	37.96°	23.68°	Rentis; Town Hall, 2-s RC	210°	4	c
SGMA+	37.98°	23.74°	Syntagma; Metro station,-7m	010°	7	b
SGMB+	37.98°	23.74°	Syntagma; Metro station, -26m	135°	3	b
SPLA+	38.00°	23.71°	Sepolia; Metro station, -13m	320°	18	c
SPLB+	38.00°	23.71°	Sepolia; Metro station, 3-s steel	320°	19	c
FILI**	38.12°	23.68°	Fili Monastery, free field	0°!	6	b
THVC+	38.32°	23.32°	Thiva; Town Hall, 3-s RC	180°	5	b
PSAR**	38.09°	23.56°	Goritsa, house, ground fl, RC	0°	6	c
MAGO**	38.08°	23.52°	Magoula, 1-story RC	0°!	6	a
STEF** N00E bad	38.17°	23.55°	Stefani, Storage, ground fl, RC	0°!	5	b
ZOFR**	38.07°	23.69°	Zofria; free field	0°	6	a
NEOK**	38.05°	23.63°	Neokista ground fl, RC	0°!	6	a

+ NOAGI station
++ NOAGI, did not record main event
** Univ. of Athens data, did not record main event
*+ .t component -90.0 from .l component
! polarity may be reversed
___ stations used in source parameter inversion

Table 2: Source Parameters for Main Event

Latitude	Longitude	Depth	Mox10^{24}dyne-cm	Duration seconds	focal mechanism STK DP	Institution/ reference
38.08	23.58	16.8			113o 39o 90o	NOAIG+
38.105	23.565	8	17.0	5	105o 35o 80o	ATHU
38.132	23.545	10	7.8		123o 35o 84o	USGS
38.119	23.605	10				PDE
37.87	23.64	15	11.0		116o 39o 81o	Harvard
			11.22			THIS STUDY

+ Papaddopoulos et. al. (personal communication, 2000)

Table 3: Source Parameters of Events

Earthquake	Latitude	Longitude	Depth	Mw! ! (M_L)!	Mo 10^{20}	fc	std	mechanism STK DP	no. stat
1999/09/07 11:56:51*	38.08	23.58	16.8	6.0 (5.4)	112200	0.45		113o 39o 90o*	10
1999/09/07 11:59:10+	38.15	23.59	5.0**	4.2	218	3.2	212		6
1999/09/07 12:00:29+	37.92	23.78	17.8	4.3	277	3.2	142		6
1999/09/07 12:01:57+	38.07	23.75	5.0**	3.7	30.4	2.4	14		2
1999/09/07 12:03:54+	38.01	23.47	5.2	___(3.5)	30.0	6.4			1
1999/09/07 12:05:12+	38.11	23.69	5.0**	4.3	197	2.7	127		4
1999/09/07 12:08:11+	37.82	23.71	5.0**	4.3	222	3.5	286		4
1999/09/07 12:16:10+	37.96	23.76	17.0	4.4	380	3.4	247		4
1999/09/07 12:20:25+	38.09	23.65	5.0**		218	5.1			1
1999/09/07 13:02:02+	38.07	23.62	5.0	3.7	20.7	3.5	27		2
1999/09/07 13:05:48+	38.13	23.51	18.2		325	3.1			1
1999/09/07 15:35:33*+	38.01	23.48	10.0	4.1(3.9)	106	4.2	188		6
1999/09/07 15:42:52*+	38.07	23.45	3.0	(3.5)	26.6	7.5			1
1999/09/07 17:19:21*	38.11	23.72	16.2	4.1(3.8)	90.8	7.0	547	114o 30o 87o	4
1999/09/07 20:44:55*	38.19	23.72	21.0	5.0(4.4)	3212	.9	28		3
1999/09/08 03:21:32*	38.09	23.83	14.1	4.1(3.7)	92.3	4.2	136		7
1999/09/08 03:35:20*	38.12	23.89	13.0	4.1(3.7)	195	7.4	1636	106o 30o 74o	3
1999/09/08 11:14:29*+	37.99	23.59	7.0	3.9(3.1)	29.5	2.9	21		2
1999/09/08 12:55:01*	38.14	23.74	19.9	(4.0)	134	2.9	61	330o 30o 30o	2
1999/09/08 13:18:21*	38.08	23.81	9.2	3.8(3.7)	27.1	3.6	44		4
1999/09/08 16:50:37*	38.19	23.91	1.4	(3.6)	48.5	4.0		113o 80o 67o	1
1999/09/08 16:54:08*	38.14	23.79	19.4	(3.5)	84.7	4.1		310o 30o 20o	1
1999/09/10 14:49:57++	38.08	23.67	9.1	4.0(3.7)	85.5	5.4	326	319o 30o 79o	10
1999/09/13 19:45:15++	38.06	23.65	9.1	3.7(3.1)	15.4	5.3	57	109o 30o -74o	10
1999/09/16 08:12:10++	38.06	23.66	7.9	3.7(3.1)	17.6	4.9	56	120o 54o 89o	10
1999/09/20 19:58:09*+	37.96	23.53	7.0	3.4(2.9)	7.29	6.9	67		9
1999/09/20 20:17:25++	37.97	23.64	8.8	2.9(2.9)	1.36	6.6	10	250o 65o-48o	7
1999/10/03 17:03:34++	38.09	23.75	9.0	4.0(3.5)	75.7	3.6	91	159o 65o 48o	9
2000/03/23 03:09:18*+	38.08	23.74	15.0	4.1(3.5)	148	4.2	202	120o 54o-89o	4

* location from Papadopoulos et al., (2000)

+ Location obtained from permanent networks in Greece and s-p arrival time intervals

++ Solution from combined data of University of Athens and National Observatory of Athens

*+ Locations routinely calculated by NOAIG from their permanent Greek network

** Depth fixed

! ! Magnitude obtained from moment/magnitude relationship Hanks and Kanamori (1979)

! Local Richter magnitude obtained from UoDA

***Moment and magnitude obtained from spectral overlay with event 1999/09/07 15:42:52

__ Mo and fc determined by all stations and with site response removed.

Table 4: Rupture Parameters

rupture parameters	
slip function	Kostrov with healing
fault geometry	depth to top of rupture 5.0 km 1.0 km; length of rupture 35.0 km 2.0 km; width of rupture 14.0 km 1.0 km;
focal mechanism	strike N274.0E 5.0^{o}, dip 45.0oN 5.0o.
Roughness	percentage is randomly selected to be either 0, 10, 20, 33, or 50% of fault surface.
Moment	constrained at 11.9 x10^{24}dyne-cm
Hypocenter	constrained to occur km from the fault edges, and the lower half of the fault
Rise time	dependent on Vr, Vh and hypo
Rupture Velocity	0.75 to 1.0 times the shear wave velocity
Healing velocity	0.8 to 1.0 times the rupture velocity
Stress drop	dependent variable derived from the Kostrov slip function and moment
Rigidity	varies with the shear wave velocity over all depths except it diminishes at the same rate as the stress drop near the surface.
Slip vector	constrained to 90.0 5.0^{o}.

Figures

Figure 1. The morphology of the Athens area, the epicenter of the main shock, and locations of stations used in this study. The circle is the 100 km extent of the demonstration PSHA, and the rectangles are the larger and smaller source zones referred to in the text.

Figure 2. Isoseismal intensity from the earthquake in Modified Mercalli Scale, and individual intensity values for the same area as specified in Table 2. The rectangles are the larger and smaller source zones referred to in the text.

Figure 3. Geology of the lower border area of Attica (modified from Katsikatsos et al., 1986), station locations, and epicenter of main event.

Figure 4. The observed spectra and the fit to calculated Brune spectra by varying moment, source corner frequency and site-specific kappa.

Figure 5. Recorded seismograms and spectra (identified by EGF) and results after the Brune source model have been deconvoled (identified by "corrected").

Figure 6. Fourier amplitude spectra for each of the 66 scenarios (dotted line), in the smaller source volume where the Athens earthquake is thought to have occurred; the plus and minus STD values of the prediction (thick dashed lines); and actual AAR recorded (thick solid line).

Figure 7. Absolute acceleration response calculated for each of the 66 scenarios (dotted line), in the smaller source volume where the Athens earthquake is thought to have occurred; the plus and minus STD values of the prediction (thick dashed lines); and actual AAR recorded (thick solid line).

Figure 8. The rupture models for scenarios that provided the best fit to observed seismograms. Model 204 is the preferred model.

Figure 9. The fit to seismograms for stations ATHA, DMKA, FIXA, and THVC for rupture model ATH008. Notice that the basic characteristics of the synthesized seismograms closely match the observed seismograms. In particular the basic waveforms, durations and frequency content match well. The frequency content is evident from the Fourier amplitude spectra.

Figure 10. Synthesized seismograms at stations that did not record the main event, but were in locations where high damage occurred.

Figure 11. Fourier amplitude spectra for 100 of the 500 scenarios calculated (dotted line), in the larger source volume where the demonstration PSHA is performed; the plus and minus STD values of the prediction (thick dashed lines); and actual AAR recorded (thick solid line).

Figure 12. The histogram (left) of AAR values at 0.5 s and the resulting hazard curve (right). The axes for the histogram extend to "extreme" values because certain combinations of rupture parameters result in high ground motions at some stations. These are indicated by vertical bars on the abscissa due to the scale being too large to see their contribution to the histogram.

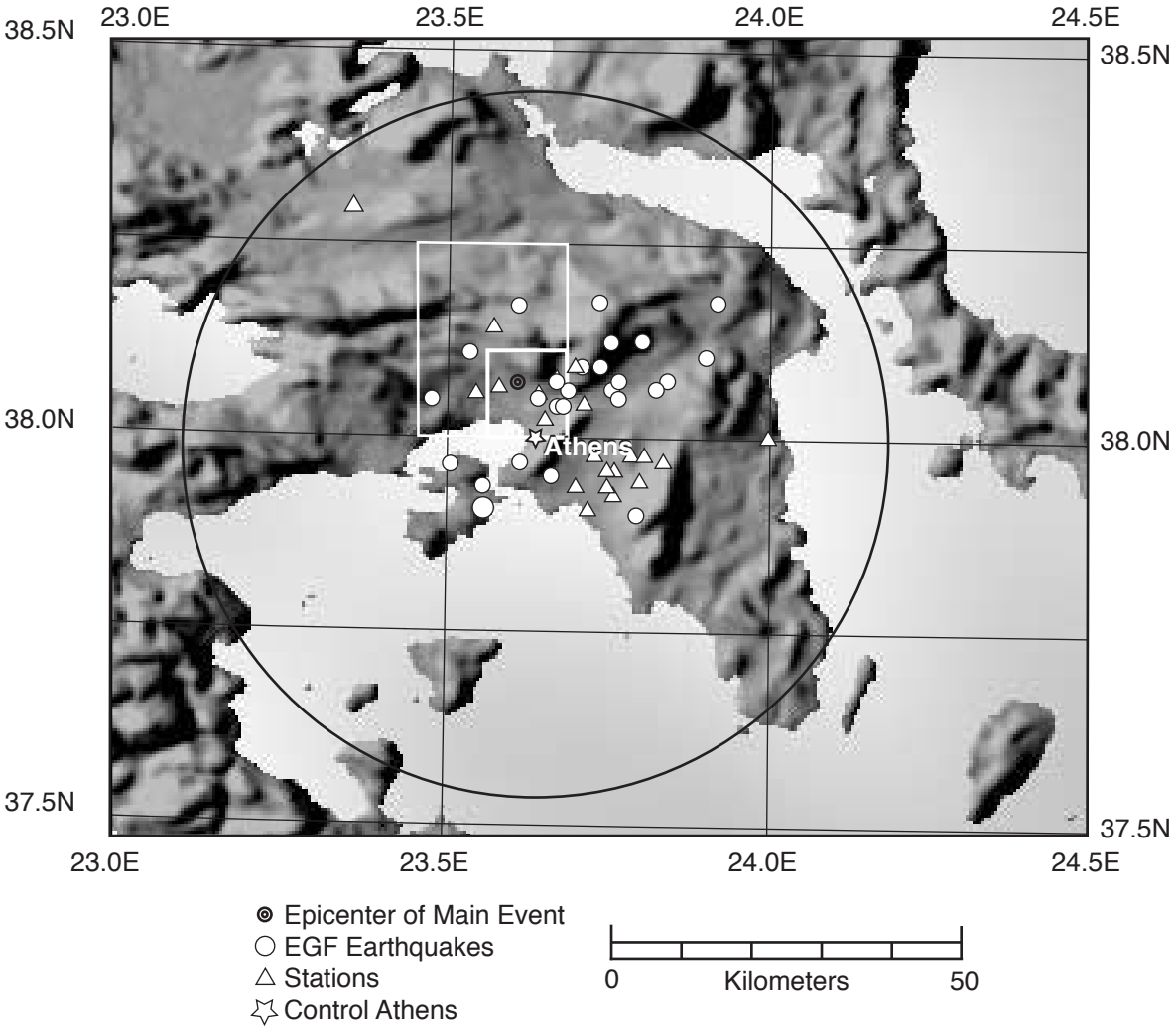

Fig 01.ai
00472
Hutchings

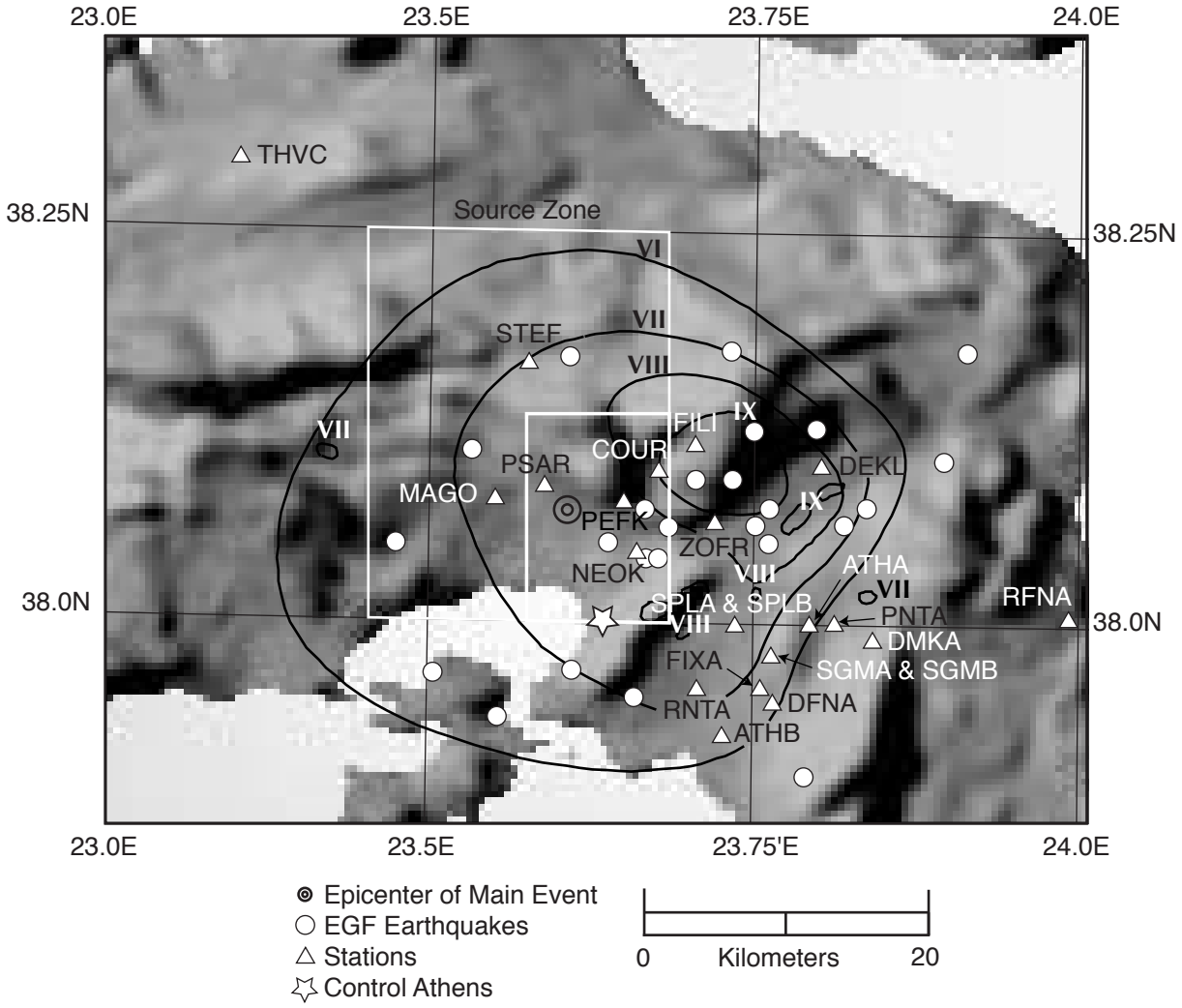

Fig 02.ai
00472
Hutchings

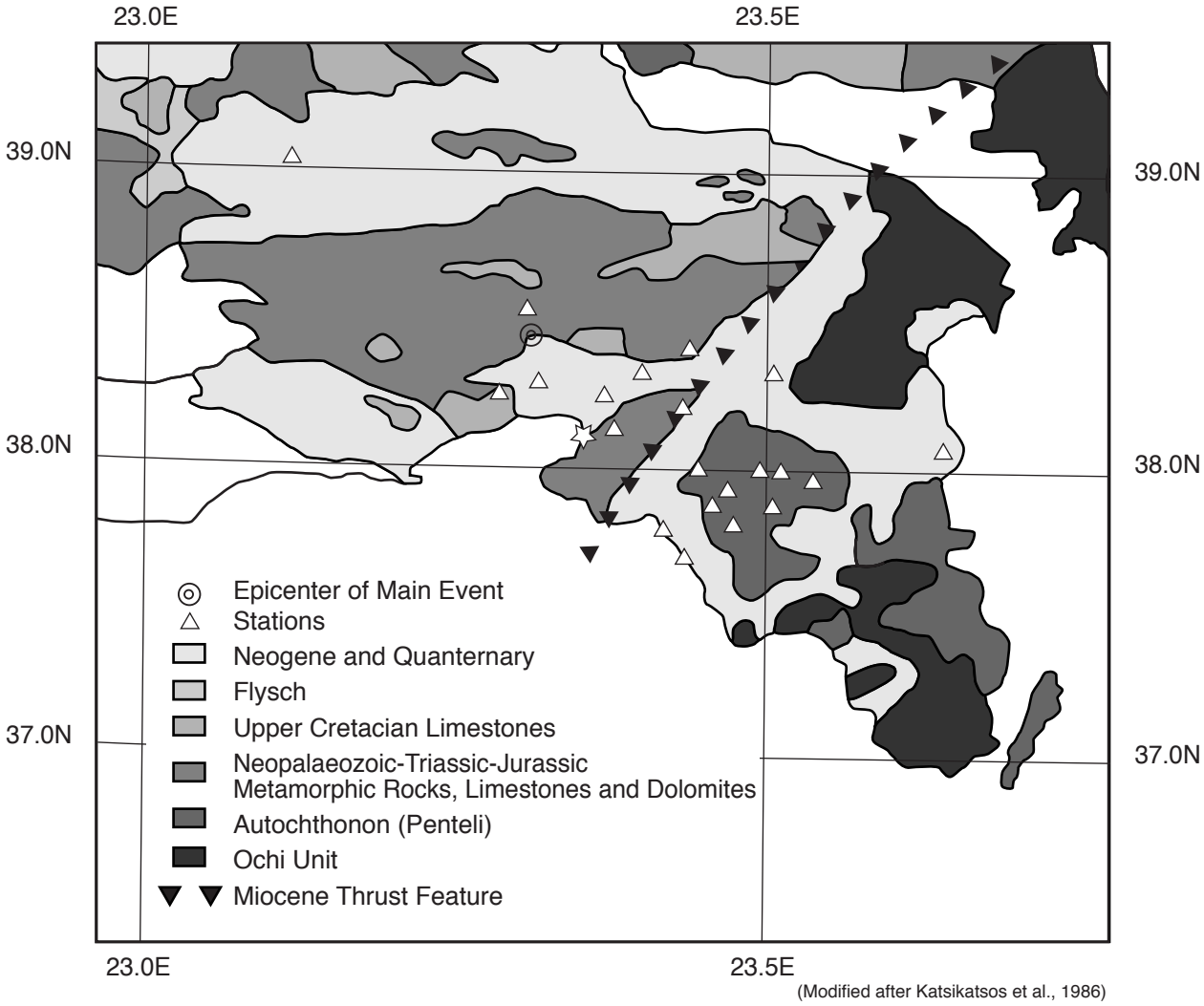

(Modified after Katsikatsos et al., 1986)

Fig 03.ai
00472
Hutchings

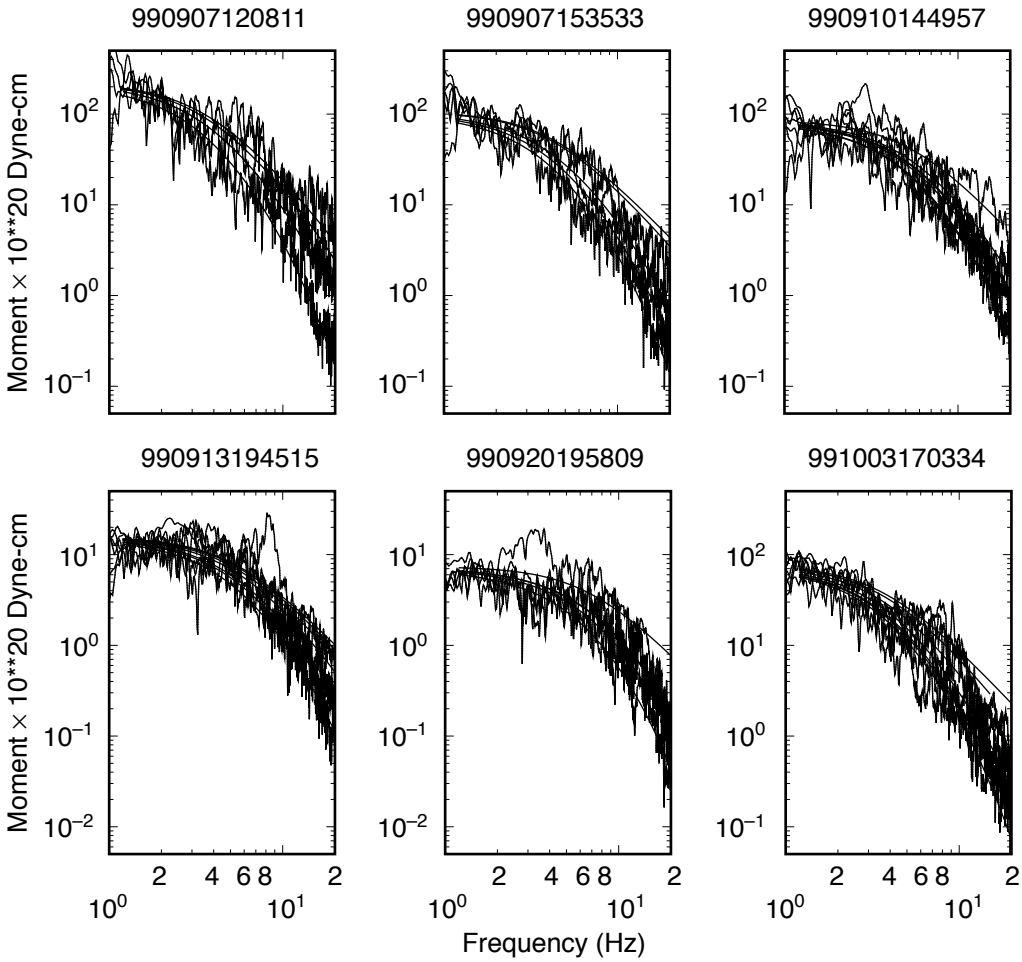

Fig 04.ai
00430
Hutchings

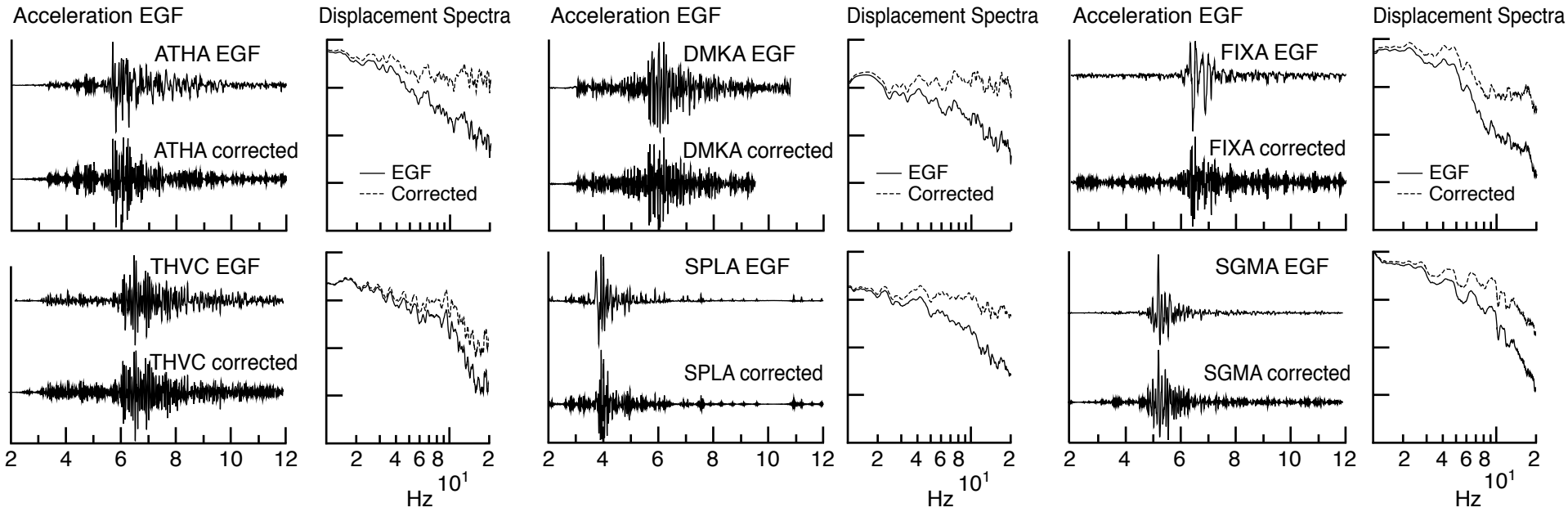

Fig 05.ai
00472
Hutchings

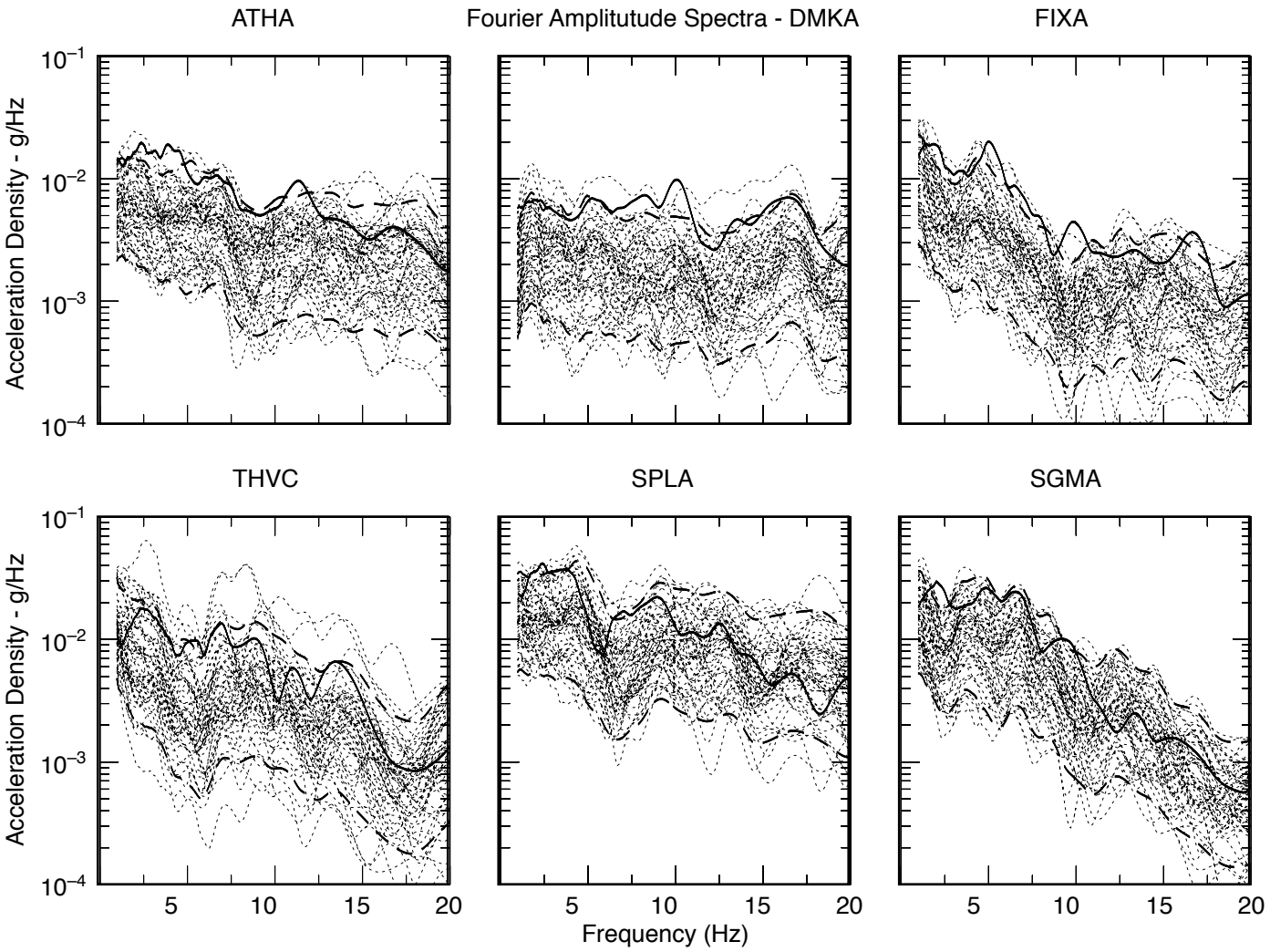

Fig 06.ai
00472]
Hutchings

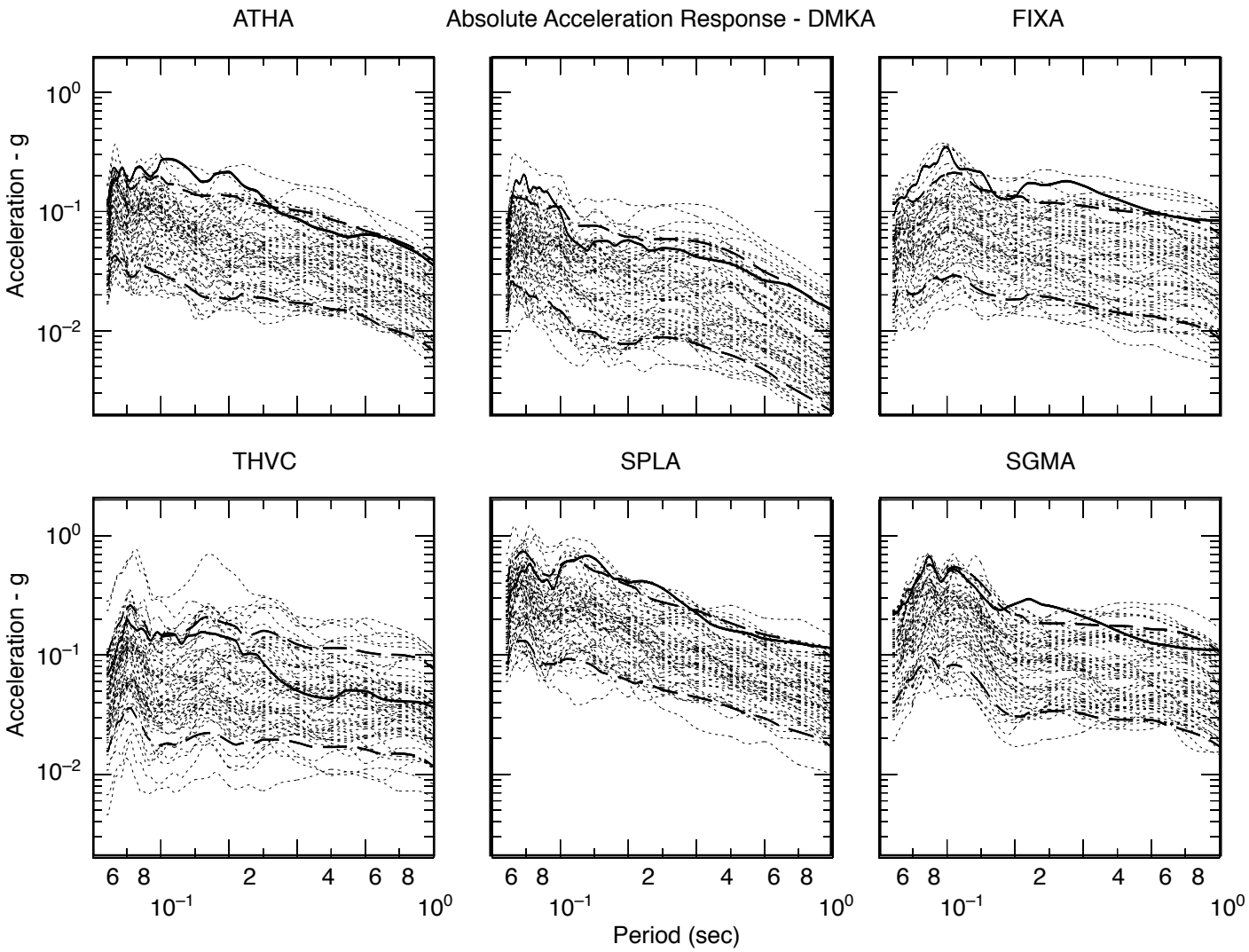

Fig 07.ai
00472
Hutchings

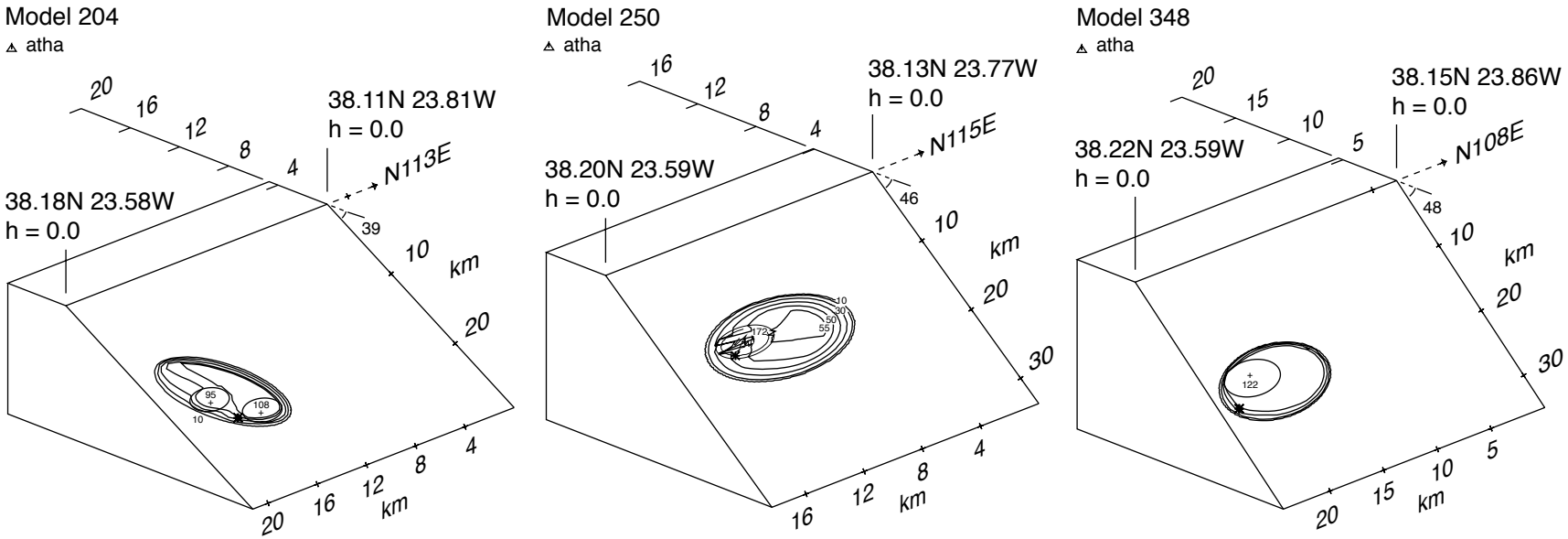

Fig 08.ai
00472
Hutchings

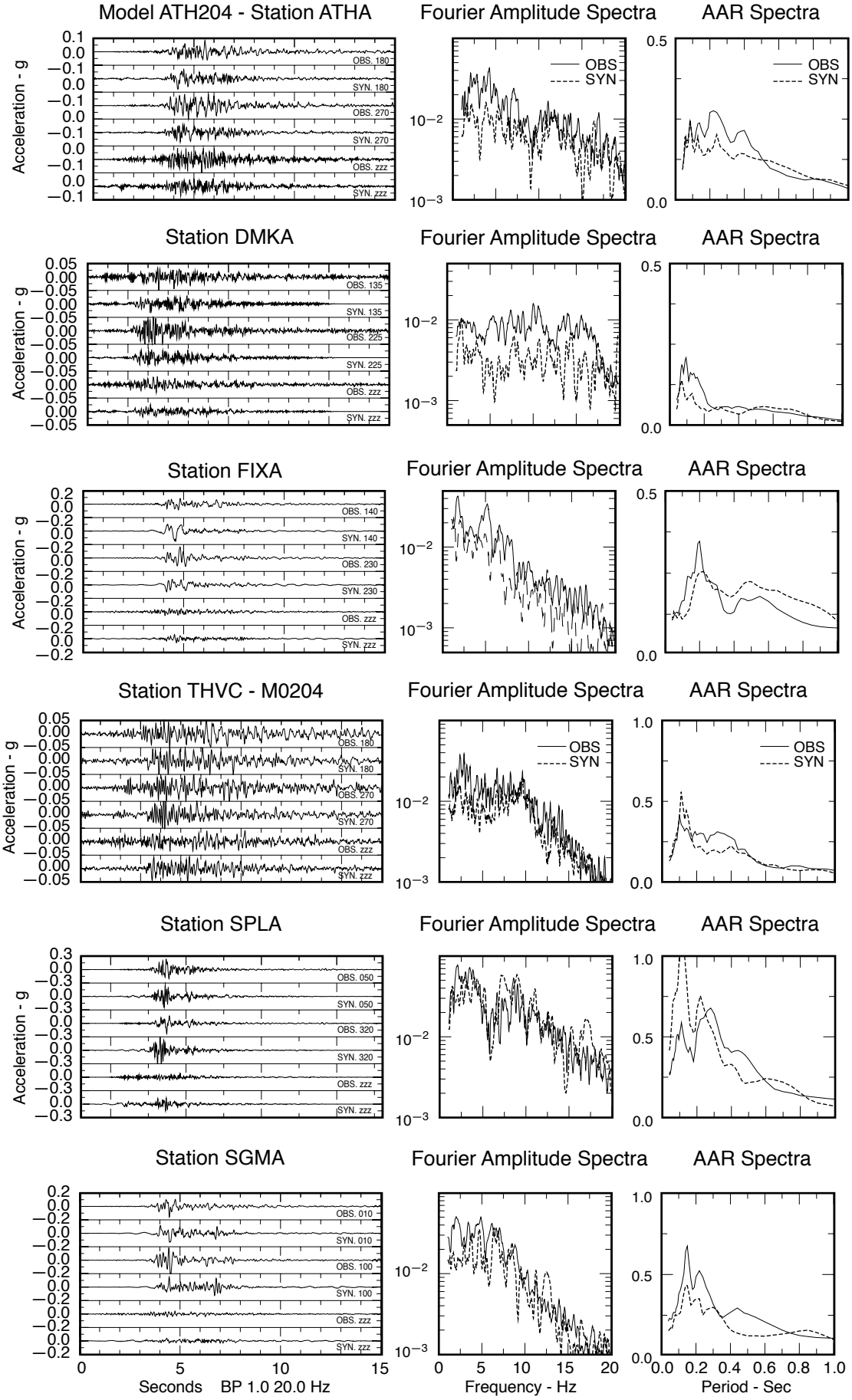

Fig 09.ai
00472
Hutchings

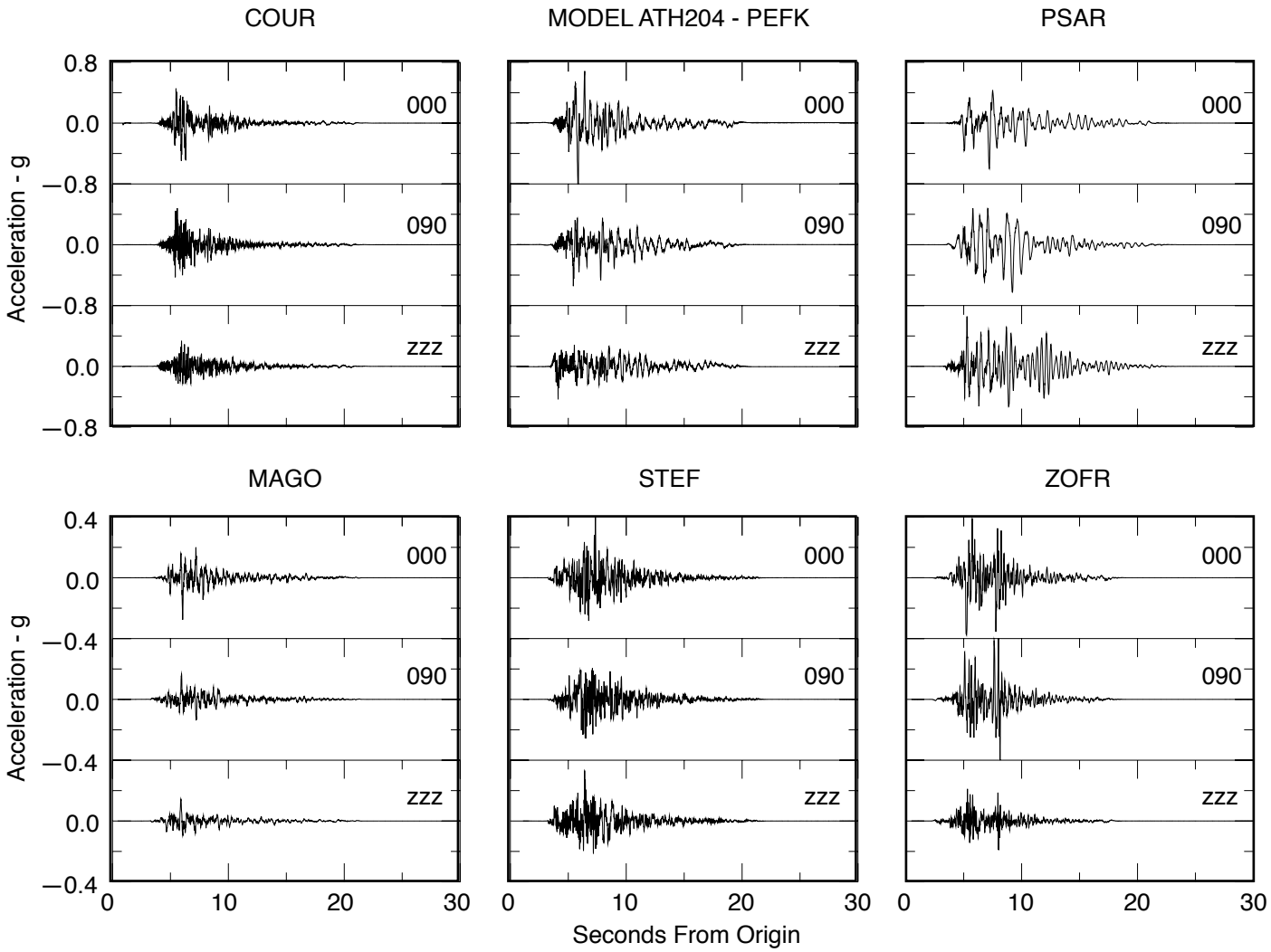

Fig 10.ai
00472
Hutchings

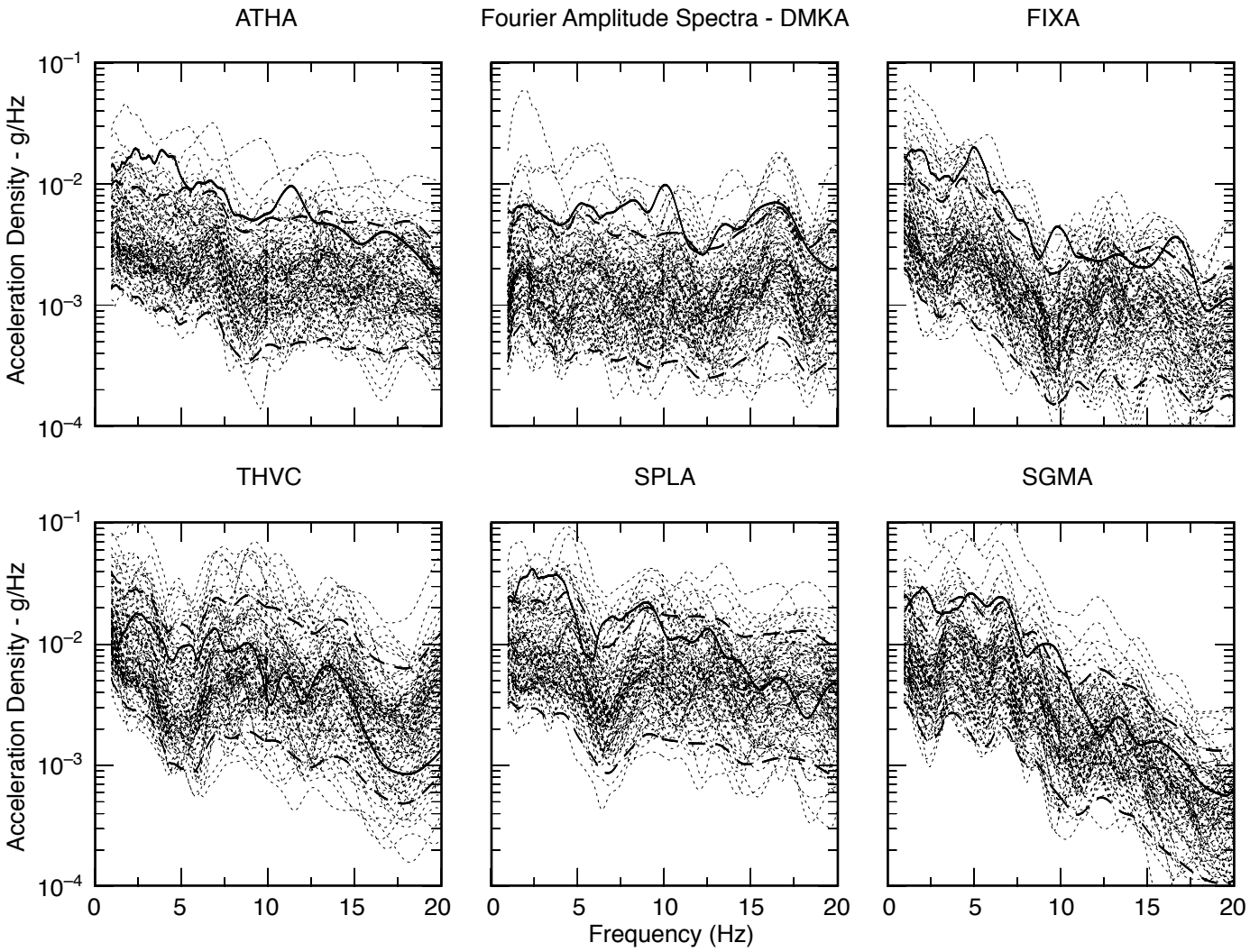

Fig 11.ai
00472
Hutchings

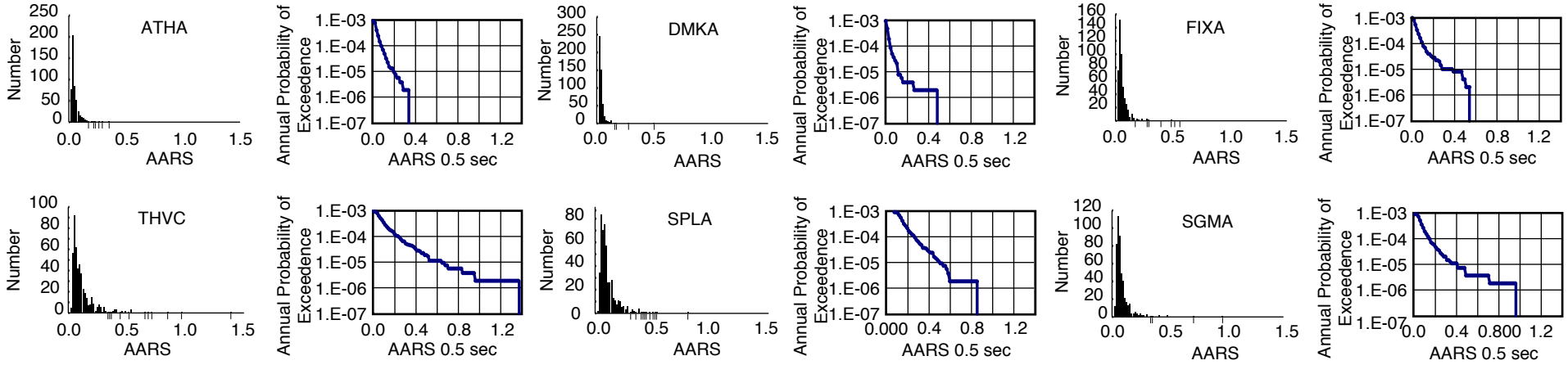

Fig 12.ai
00472
Hutchings